Check for updates

The organization of serotonergic fibers in the Pacific angelshark brain: neuroanatomical and supercomputing analyses

Skirmantas Janušonis[1]*, Ralf Metzler[2] and Thomas Vojta[3]

[1]Department of Psychological and Brain Sciences, University of California, Santa Barbara, Santa Barbara, CA, United States, [2]Institute of Physics and Astronomy, University of Potsdam, Potsdam, Germany, [3]Department of Physics, Missouri University of Science and Technology, Rolla, MO, United States

Serotonergic axons (fibers) are a universal feature of all vertebrate brains. They form meshworks, typically quantified with regional density measurements, and appear to support neuroplasticity. The self-organization of this system remains poorly understood, partly because of the strong stochasticity of individual fiber trajectories. In an extension to our previous analyses of the mouse brain, serotonergic fibers were investigated in the brain of the Pacific angelshark (*Squatina californica*), a representative of a unique (ray-like) lineage of the squalomorph sharks. First, the fundamental cytoarchitecture of the angelshark brain was examined, including the expression of ionized calcium-binding adapter molecule 1 (Iba1, AIF-1) and the mesencephalic trigeminal nucleus. Second, serotonergic fibers were visualized with immunohistochemistry, which showed that fibers in the forebrain have the tendency to move toward the dorsal pallium and also accumulate at higher densities at pial borders. Third, a population of serotonergic fibers was modeled inside a digital model of the angelshark brain by using a supercomputing simulation. The simulated fibers were defined as sample paths of reflected fractional Brownian motion (FBM), a continuous-time stochastic process. The regional densities generated by these simulated fibers reproduced key features of the biological serotonergic fiber densities in the telencephalon, a brain division with a considerable physical uniformity and no major "obstacles" (dense axon tracts). These results demonstrate that the paths of serotonergic fibers may be inherently stochastic, and that a large population of such paths can give rise to a consistent, non-uniform, and biologically-realistic fiber density distribution. Local densities may be induced by the constraints of the three-dimensional geometry of the brain, with no axon guidance cues. However, they can be further refined by anisotropies that constrain fiber movement (e.g., major axon tracts, active self-avoidance, chemical gradients). In the angelshark forebrain, such constraints may be reduced to an attractive effect of the dorsal pallium, suggesting that anatomically complex distributions of fiber densities can emerge from the interplay of a small set of stochastic and deterministic processes.

KEYWORDS

5-hydroxytryptamine (5-HT), serotonin, axon, density, shark, stochastic process, fractional Brownian motion, supercomputing

1 Introduction

Serotonergic axons (fibers) have been found in all studied vertebrate brains, where they form dense meshworks in many brain regions. Their ubiquity and morphological similarity across distant phylogenetic branches (cartilaginous and bony fishes, amphibians, sauropsids, mammals) suggests that they are an obligatory component of neural tissue, independent of clade-specific cytoarchitectonic specializations (e.g., the mammalian cerebral cortex) (Parent, 1981; Lillesaar, 2011; Lozano et al., 2020; Yip et al., 2020; Awasthi et al., 2021; Bhat and Ganesh, 2023; Fujita et al., 2023; Biradar and Ganesh, 2024). Serotonergic fibers store and release serotonin (5-hydroxytryptamine, 5-HT) that can be detected by a large class of receptors (Bockaert et al., 2006), through volume or wiring neurotransmission (Papadopoulos et al., 1987; Smiley and Goldman-Rakic, 1996; Gianni and Pasqualetti, 2023; Zhang et al., 2025). Some evidence exists that serotonin can directly modulate the membrane lipid bilayer (Dey et al., 2021) and can even be transported into cells and their organelles by facilitated diffusion (Andrews et al., 2022). Fundamentally, serotonergic signaling appears to support neuroplasticity (Lesch and Waider, 2012; Teissier et al., 2017; Cazettes et al., 2021; Ogelman et al., 2024; Page et al., 2024). No major neuroanatomical or electrophysiological defects have been detected in mice that cannot synthesize serotonin in the central nervous system (CNS), but these mice do show innervation and behavioral alterations (Migliarini et al., 2013; Montalbano et al., 2015; Mosienko et al., 2015). Notably, serotonergic fibers have no analogs in current artificial neural network architectures (Lee et al., 2022), where the loss of plasticity in deep continual learning remains a challenging problem (Dohare et al., 2024).

Recent studies have revealed a great diversity of transcriptional programs in the mouse serotonergic neurons (Okaty et al., 2019; Ren et al., 2019; Okaty et al., 2020) and also have shown that serotonergic fibers can regenerate in adult mammalian brains, with new trajectories (Hawthorne et al., 2011; Jin et al., 2016; Kajstura et al., 2018; Cooke et al., 2022). Most serotonergic axons appear to be unmyelinated, but myelinated serotonergic fibers have been reported in rodents and primates (Azmitia and Gannon, 1983; Westlund et al., 1992).

The processes that assemble serotonergic fibers into brain region-specific densities remain poorly understood. In mammals, the serotonergic fibers originate in the brainstem raphe nuclei and as a population reach all brain regions (Jacobs and Azmitia, 1992; Hornung, 2003). Different raphe nuclei and their subdivisions appear to preferentially target specific brain regions, but these projections are not fully segregated (Vertes, 1991; Vertes et al., 1999; Ren et al., 2018; Ren et al., 2019). In embryonic development, serotonergic fibers form some well-defined fascicles that carry fibers to the forebrain (Lidov and Molliver, 1982; Wallace and Lauder, 1983; Aitken and Tork, 1988; Slaten et al., 2010). However, these fascicles tend to travel along existing axon tracts produced by other, non-serotonergic axons (e.g., the medial forebrain bundle, the fasciculus retroflexus), that may serve only as contact guides (Lidov and Molliver, 1982; Wallace and Lauder, 1983; Jacobs and Azmitia, 1992). Growing serotonergic axons form specific adhesion structures on other neurites *in vitro* (Hingorani et al., 2022). A number of factors have been implicated in the growth, distribution, and survival of serotonergic fibers: the transcription factors Lmx1b and Pet-1 (Donovan et al., 2019; Kitt et al., 2022), protocadherin-αC2 (Chen et al., 2017; Katori et al., 2017), neurexins (Cheung et al., 2023), neuritin (Shimada et al., 2024), S100β (Azmitia and Whitaker-Azmitia, 1991; Whitaker-Azmitia, 2001), the brain-derived neurotrophic factor (BDNF; Mamounas et al., 1995), serotonin itself (Migliarini et al., 2013; Nazzi et al., 2019; Nazzi et al., 2024), and others (Kiyasova and Gaspar, 2011). However, the relative roles of these factors (e.g., essential, supportive, injury-related), as well as their interactions, require further research. For example, transgenic mice lacking S100β appear to have no major defects in the development of serotonergic neurons (Nishiyama et al., 2002), and questions remain about the serotonin levels required to significantly alter serotonergic fiber densities (Migliarini et al., 2013; Donovan et al., 2019).

We have recently introduced a novel approach that treats serotonergic fibers as paths of spatial stochastic processes, with no axon guidance cues (Janušonis and Detering, 2019; Janušonis et al., 2020). Such processes are random walk-like, but they can evolve in continuous time and have a complex autocorrelative structure. In particular, the trajectories of serotonergic fibers can be modeled as sample paths of fractional Brownian motion (FBM), a major generalization of normal Brownian motion that allows correlations between steps and exhibits long-range dependence (Mandelbrot and Van Ness, 1968; Biagini et al., 2010). Reflected FBM, a further extension necessary for computer simulations in bounded shapes (such as a brain), has been introduced only recently (Wada and Vojta, 2018; Guggenberger et al., 2019; Vojta et al., 2020). We have shown that FBM-fibers in a three-dimensional model of the mouse brain can automatically reproduce some regional serotonergic fiber densities described by neuroanatomical studies (Janušonis et al., 2023).

The proposed stochastic models are predictive in that they seek to simulate regional serotonergic fiber densities in any vertebrate brains – extant, extinct, or hypothetical. The results obtained in the mouse brain are promising (Janušonis et al., 2020; Janušonis et al., 2023), but they require validation in vertebrate brains that have different shapes and express different genes. Diverse brain shapes are important because reflected FBM is sensitive to the geometry of the bounding borders (Janušonis et al., 2020; Vojta et al., 2020). Since FBM has "memory," this effect is not fully local and reflects the history of the fiber trajectory. Diverse genomes are important because the model assumes that the key properties of regional fiber densities can be predicted without detailed knowledge of axon guidance mechanisms. It should be noted that the model does not rule out such mechanisms and can include them as additional "forces" [e.g., modeled by "effective potentials" (Rizzo et al., 2013)] to further refine predictions. However, these extensions require quantitative definitions of such "forces" in the brain space, which are difficult to obtain from current experimental data.

Fish brains meet these two criteria. In particular, the extant cartilaginous fishes (sharks, skates, rays) produce a remarkable diversity of brain shapes (Yopak, 2012) and nearly maximize the phylogenetic distance to the mammals. In addition, the distributions of neurons in shark telencephala are much more uniform compared to those in mammalian telencephala which contain many differentiated cortical and subcortical structures. Therefore, a shark telencephalon can serve as a natural model of neural tissue that possesses a considerable degree of physical

homogeneity, up to the natural brain borders. In computer simulations, these borders (the pial and ependymal surfaces) can be unambiguously modeled as impenetrable boundaries. Such biomechanical homogeneity does not imply chemoarchitectonic or functional homogeneities (unrealistic for any functional brain), but it eliminates the problem of complex physical "obstacles" (e.g., dense anatomical nuclei or axon tracts). These "obstacles" may differ in their permeability to serotonergic fibers (Janušonis et al., 2020) and viscoelastic properties (Chaudhuri et al., 2020; Antonovaite et al., 2021). In computer simulations, they introduce uncertainties and require careful treatment (Janušonis et al., 2020; Janušonis et al., 2023). It should be noted that nearly perfectly uniform environments can be created in cell cultures (Hingorani et al., 2022); however, these systems differ strongly from the natural brain environment, physically and chemically. In particular, they are usually two-dimensional, which has a major impact on the normal behavior of growing axons (Santos et al., 2020).

The extant sharks comprise around 500 species (Compagno et al., 2005) that can be divided into two superorders, the squalomorph sharks (Squalomorphii) and the galeomorph sharks (Galeomorphii; this group includes the great white shark). Relative to body size, the squalomorph sharks tend to have smaller brains (Striedter and Northcutt, 2020), with fewer differentiated cell masses (Butler and Hodos, 2005), which makes them convenient for the purpose of this study. Among several squalomorph species readily available along the coast of Southern California, we selected the Pacific angelshark (*Squatina californica* Ayres, 1859), a representative of the angelshark order (Squatiniformes).

The angelshark body is superficially similar to that of rays; paleontological evidence suggests that this lineage dates back to the Late Jurassic (López-Romero et al., 2020; Maisey et al., 2020). Historically, angelsharks have been called "angels," "monks," and "bishops," with colorful descriptions dating back to at least the 16th century (McCormick et al., 1963; Compagno et al., 2005). The Pacific angelshark is found along the continental shelf of the east Pacific, typically on sandy flats (Compagno et al., 2005). To our knowledge, angelshark brains have been studied only at the gross anatomical level (Striedter and Northcutt, 2020), with no published reports on their cytoarchitecture or chemoarchitecture.

In this report, we first describe the basic neuroanatomy of the Pacific angelshark brain and visualize its serotonergic fibers. We then build its three-dimensional model, populate it with growing fibers modeled as reflected FBM paths, and use a supercomputing simulation to generate regional fiber densities. Finally, we compare these simulated densities with the biological fiber densities in the angelshark brain.

2 Materials and methods

2.1 Animals and brain preparation

Three adult Pacific angelshark *(Squatina californica)* specimens (two females, one male) were collected in 2017 from the UCSB Parasitology laboratory, with a post-mortem interval of 0–2 h (after euthanasia with MS-222). The brains of the specimens were immediately removed, rinsed in 0.1 M phosphate-buffered saline (PBS, pH 7.2), and immersion-fixed in phosphate-buffered 4% paraformaldehyde at 4°C overnight. The fixed brains were immersed in 30% sucrose in PBS at 4°C for 2 days, transferred to a cryoprotectant solution (30% sucrose, 1% (w/v) polyvinylpyrrolidone (PVP-40), and 30% (v/v) ethylene glycol in PBS) at 4°C for 2 days, and then moved (in cryoprotectant) to −20°C for indefinite storage. All procedures have been approved by the UCSB Institutional Animal Care and Use Committee.

2.2 Brain sectioning

The brains stored in cryoprotectant were moved from −20°C to 4°C for 1 day and then transferred to 30% sucrose in PBS at 4°C for 2 days. They were divided into two rostro-caudal pieces, each of which was embedded in 20% gelatin (type A; Thermo Scientific #61199-5000) in a Peel-Away mold. An insect pin was pushed through the mold in the rostro-caudal orientation over the dorsal surface of the brain for physical support and as a fiducial marker for further alignment (Janušonis et al., 2023). After 1 h at 4°C, the gelatin blocks were removed, trimmed, and immersed for 3 h in undiluted formalin with 20% sucrose at room temperature. They were sectioned coronally from the rostral pole through the rostral myelencephalon at 40 μm thickness on a freezing microtome into 96-well trays with PBS. In order to avoid distance distortions in the rostro-caudal axis, damaged or missing sections were marked with empty wells. The processing of the two blocks was staggered to ensure the same exposure times.

2.3 The serial section set

A subset of the complete section series from one female brain was used to visualize cell bodies and major fiber tracts. The same set was used to build a 3D-model of the Pacific angelshark brain for supercomputing simulations (See section "2.7. The brain model").

One-fourth of all ordered sections (with a constant rostro-caudal step of 160 μm) were mounted onto gelatin/chromium-subbed glass slides and allowed to air-dry. They were used to acquire three sets of images. First, the sections were imaged uncoverslipped in bright-field with a 1 × objective. In these images, neural tissue is uniformly dark, which supports efficient capture of outer and inner (e.g., ventricle) brain contours. Next, the sections were briefly dipped in water and, while wet, were again imaged uncoverslipped with the same 1 × objective. It revealed major fiber tracts that appeared dark against the remaining light tissue (due to light refraction). Finally, the same sections were Nissl-stained to reveal the basic cytoarchitecture of the neural tissue. They were rehydrated, stained with 0.25% thionine acetate (Millipore-Sigma #861340) for 13 sec, dehydrated in a graded series of ethanols, differentiated in 95% ethanol with 1.1% glacial acetic acid for 4 min, further dehydrated in absolute ethanol, cleared (defatted) in Xylenes, and coverslipped with Permount.

The remaining unmounted sections were moved to cryoprotectant at 4°C (with several changes over a few days) and eventually stored in 20 mL glass scintillation vials at –20°C until further processing.

2.4 Iba1 immunohistochemistry

Some free-floating sections were stained for ionized calcium-binding adapter molecule (Iba1), also known as allograft inflammatory factor 1 (AIF-1) (all procedures were at room temperature unless otherwise indicated). Sections in cryoprotectant were allowed to slowly equilibrate to 4°C and thoroughly rinsed in PBS. They were blocked in 2% normal donkey serum (NDS; Jackson ImmunoResearch #017-000-121) for 30 min and incubated in rabbit anti-Iba1 IgG (1:500; FUJIFILM Wako Pure Chemical Corporation #019-19741) with 2% NDS and 0.3% Triton X-100 (TX) in PBS for 2 days at 4°C on a shaker. The specificity of the anti-Iba1 antibody has been validated in previous studies (Wake et al., 2009; Bifari et al., 2017; Janušonis, 2018). The sections were rinsed in PBS (three times, 10 min each), incubated in AlexaFluor 488-conjugated donkey anti-rabbit IgG (1:1000; ThermoFisher Scientific #A-21206) with 2% NDS in PBS for 90 min, rinsed in PBS (three times, 10 min each), mounted onto gelatin/chromium-subbed glass slides, allowed to air-dry in the dark, and coverslipped with the ProlongGold antifade mountant with the DNA stain DAPI (Thermo Fisher Scientific #P36931).

2.5 5-HT immunohistochemistry

Sections at representative coronal levels were stained for 5-HT to visualize serotonergic fibers (all procedures were at room temperature unless otherwise indicated). Sections in cryoprotectant were allowed to slowly equilibrate to 4°C and thoroughly rinsed in PBS. They were blocked in 3% NDS for 30 min and incubated in goat anti-5-HT IgG (1:500; ImmunoStar #20079) with 2% NDS and 0.3% Triton X-100 (TX) in PBS for 2 days at 4°C on a shaker. They were rinsed in PBS (three times, 10 min each), incubated in Cy3-conjugated donkey anti-goat IgG (1:400; Jackson ImmunoResearch #705-165-147) with 2% NDS in PBS for 90 min, rinsed in PBS (three times, 10 min each), mounted onto gelatin/chromium-subbed glass slides, allowed to air-dry in the dark, and coverslipped with the ProlongGold antifade mountant with DAPI. Some sections were double-stained for 5-HT and Iba1. The procedure was the same, with the addition of the rabbit anti-Iba1 antibody and the AlexaFluor 488-conjugated donkey anti-rabbit antibody in the primary and secondary antibody steps, respectively (at the concentrations given in section "2.4. Iba1 immunohistochemistry").

2.6 Microscopy and imaging

Bright-field and epifluorescence imaging was performed on a Zeiss AxioImager Z1 system, using 1 × (Plan-Neofluar, NA = 0.025), 5 × (EC Plan-Neofluar, NA 0.16), and 10 × (Plan-Apochromat, NA 0.45) objectives. Confocal imaging was performed on a Leica SP8 resonant scanning confocal system in three channels (Cy3, AlexaFluor 488, DAPI), using a 63 × oil objective (NA 1.40) with the xy-resolution of 59 nm/pixel and the z-resolution of 299 nm/optical section. The figures show maximum-intensity projections.

All images were captured at light intensities and exposures that maximized the dynamic range of the camera sensors (i.e., such that the histograms covered the largest available range of values, with no saturated pixels inside tissue borders). In post-processing in Adobe Photoshop (versions 25 and 26), the darkest pixel values were set to pure black and the brightest ones to pure white in each color channel (with linear or near-linear mapping between these values). Some grayscale images were inverted, as described in the figure captions. All adjustments were applied to the entire image.

2.7 The brain model

The images of the dry sections (separated by a constant rostro-caudal step of 160 μm; See section "2.3. The serial section set") from the rostral pole to the mid-mesencephalon level were imported into the Reconstruct software (SynapseWeb) and aligned in the rostro-caudal axis, as described in our previous publications (Flood et al., 2012; Janušonis et al., 2023). Outer and inner brain contours were outlined in Photoshop by an expert neuroanatomist, imported into Wolfram Mathematica 14 (Wolfram Research, Inc.), and converted to point (x, y) arrays, as previously described (Janušonis et al., 2020; Janušonis et al., 2023).

Briefly, each closed contour was read as an ordered set of points, smoothed, bilaterally symmetrized, and transformed to an $N \times 3$ matrix (where N is the number of the rows). The rows represented the consecutive y-coordinates (with no gaps), from the most dorsal level to the most ventral level of the contour. Each row contained three values: its y-coordinate and the leftmost and rightmost x-coordinates of the shape enclosed by the contour (at this y-coordinate). Both x- and y-coordinates were integers. Since this format cannot capture concavities oriented in the dorsoventral direction, they were coded as separate contours representing "forbidden" regions in the corresponding convex shape. In this two-dimensional (2D)-integer grid, the side of each square cell represented the distance of 12.5 μm in the physical brain.

The most caudal section (at the mid-mesencephalon level) was cloned 10 times to reduce distortions at the unnatural caudal border (the biological brain continues further and smoothly transitions to the spinal cord; the entire organ ends only at the caudal point of the spinal cord). This approach was justified by the relatively constant shape of the biological brain at this level (the large tectum and the tegmentum).

In the next step, a three-dimensional brain model was built from the section stack. Each two-dimensional section (with the virtual thickness of 160 μm) was subdivided into 13 thinner virtual sections (around 12.5 μm in thickness each) using linear interpolation. This produced a simulation grid with cells (voxels) that were cubes with sides corresponding to 12.5 μm in the physical brain.

2.8 The supercomputing simulation

The supercomputing simulation was performed as described in our previous study in the mouse brain (Janušonis et al., 2023), with some modifications.

The fiber densities were produced by 4800 growing fibers that were randomly seeded in the most caudal coronal section

(representing the mid-mesencephalon). This decision was motivated by the tegmental location of the rostral raphe nuclei in all vertebrates (Butler and Hodos, 2005; Lillesaar, 2011) and by the presence of serotonergic neurons in the tectum of some cartilaginous fish species (Stuesse et al., 1991). Fibers were not seeded at more rostral levels (including the hypothalamus); however, relative fiber densities are insensitive to the location of the origin points after sufficiently long simulation times. Each fiber was represented by a three-dimensional path of a discrete, superdiffusive FBM (Qian, 2003): its trajectory moved according to the recursion relation $r_{n+1} = r_n + \xi_n$, where r_n is the three-dimensional walker position, and the steps (increments) ξ_n are a three-component discrete fractional Gaussian noise. The statistically-independent x, y, and z components of ξ_n were Gaussian random numbers with mean zero and variance σ^2. Each component had long-range correlations between its steps; the corresponding noise covariance function between steps m and $m + n$ was given by $\xi_{i,m}\xi_{j,m+n} = \frac{1}{2}\delta_{ij}\sigma^2 \left[|n+1|^{2H} - 2|n|^{2H} + |n-1|^{2H}\right]$, where H is the Hurst index, δ_{ij} is the Kronecker delta, and $i, j = x, y, z$ denotes the three space dimensions. The Fourier-filtering method was employed to generate these long-range correlated, stationary random numbers on the computer (Makse et al., 1996; Wada and Vojta, 2018; Vojta et al., 2020). The Hurst index was set at 0.8, based on our previous research in the mouse brain (Janušonis et al., 2020; Vojta et al., 2020; Janušonis et al., 2023), and the root mean-squared step size was set to $\sigma = 0.2$ grid units, corresponding to 2.5 μm in the physical brain (considerably less than the diameter of a single neuron). Each trajectory was composed of $2^{25} \approx 33.6$ million walk-steps. The length of the trajectories was sufficient for the relative densities to reach a steady state.

If a growing fiber encountered a boundary (i.e., an outer or inner contour), it was "reflected" by it (i.e., it was not allowed to cross it). Several reflection rules are available in simulations. They differ in computational complexity, but this choice has virtually no effect on simulation results, as we have shown previously (Vojta et al., 2020). In this simulation, a step that would push the leading fiber end into the forbidden region was simply not carried out. The entire sections at the most rostral and caudal levels were treated as reflecting boundaries.

After the simulation, the obtained densities were evaluated in non-overlapping cubes (composed of $2 \times 2 \times 2$ grid cells, to suppress noise and achieve more robust estimates). The local density (d_s) was determined by counting the total number of random-walk segments inside each cell. These local densities were normalized to the total sum of unity in the entire three-dimensional brain volume, to make the results independent of the arbitrarily chosen trajectory length. To facilitate comparisons between the simulated fiber densities and actual fiber densities in immunostained sections, the raw simulation densities were transformed to "optical densities" using the transformation $d_o = \exp(-kd_s)$ (Janušonis et al., 2020; Janušonis et al., 2023), with an empirically optimized k-value ($k = 10^{8.2}$). This transformation constrained density values to a finite interval (from zero to one), with lower ("darker") values corresponding to higher fiber densities. Graphical density maps were produced in Wolfram Mathematica 14 using the built-in "GrayTones" color function.

All supercomputing simulations were written in Fortran 2018 and carried out on the Pegasus cluster at the Missouri University of Science and Technology, using parallel processing on several hundred CPU cores.

3 Results

3.1 Anatomical features of the Pacific angelshark brain

The Pacific angelshark (Figure 1A) is a typical representative of the angelshark family (Squatinidae) and has a flattened body, dorsally-positioned eyes, and relatively large spiracles typical for bottom-dwelling shark species (Compagno et al., 2005). Its brain is relatively small compared to the body size (Figures 1B, C), as expected for squalomorph sharks (Striedter and Northcutt, 2020). Considering that some of the major brain divisions (e.g., the telencephalon or cerebellum) can become greatly enlarged in various elasmobranch species (Hofmann and Northcutt, 2012; Yopak, 2012; Yopak et al., 2019; Striedter and Northcutt, 2020), none of these divisions appears "exaggerated" in the angelshark brain (Figure 1B).

The basic neuroanatomy of the angelshark brain was captured in coronal sections that were imaged stained with a Nissl dye (to reveal cell bodies) and prior to the staining (to reveal highly refractive structures) (Figure 2). The most prominent differentiated structure in the telencephalon was the area superficialis basalis (asb), a consistent feature in elasmobranch brains (Smeets et al., 1983; Smeets, 1998; Hofmann and Northcutt, 2012). The telencephalon had no strongly refractive structures, with the exception of the fasciculus basalis telencephali (fbt), the intensity of which became stronger as it approached the optic tract in the diencephalon. In the diencephalon, extremely strong refraction was associated with the optic chiasm and the optic tract, confirming that the imaging correctly visualized major axon tracts. In stark contrast to the telencephalon, the entire mesencephalon and myelencephalon were strongly refractive, suggesting the presence of many densely packed axon tracts in this brain division. This observation was again consistent with fundamental anatomy, considering that cranial nerves III-XII, a universal input/output system in the vertebrate clade (Striedter and Northcutt, 2020), are directly associated with the brainstem.

The highly refractive structures were likely myelinated (de Bellard, 2016; Zalc, 2016; Verkhratsky et al., 2022), but the presence of myelin-associated proteins [e.g., myelin protein zero (MPZ)] was not directly examined in this study. Based on studies in other shark species, the angelshark telencephalon should contain several well-defined projections (Smeets, 1998; Hofmann and Northcutt, 2012). However, the majority of projections within the telencephalon are unmyelinated and loosely organized (Smeets et al., 1983; Smeets, 1998). The fbt is a notable exception and contains myelinated axons, as has been reported in another squalomorph species, the spiny dogfish (*Squalus acanthias*) (Smeets, 1998). In the angelshark, the fbt was located just ventral to the caudal asb (Figures 3A–C). The asb contributes axons to the fbt (Hofmann and Northcutt, 2012), but probably not to the extent that was previously assumed (Smeets, 1998).

A cluster of giant (around 100 μm in length) cells were present in the roof of the tectal ventricle (Figure 3D). These cells
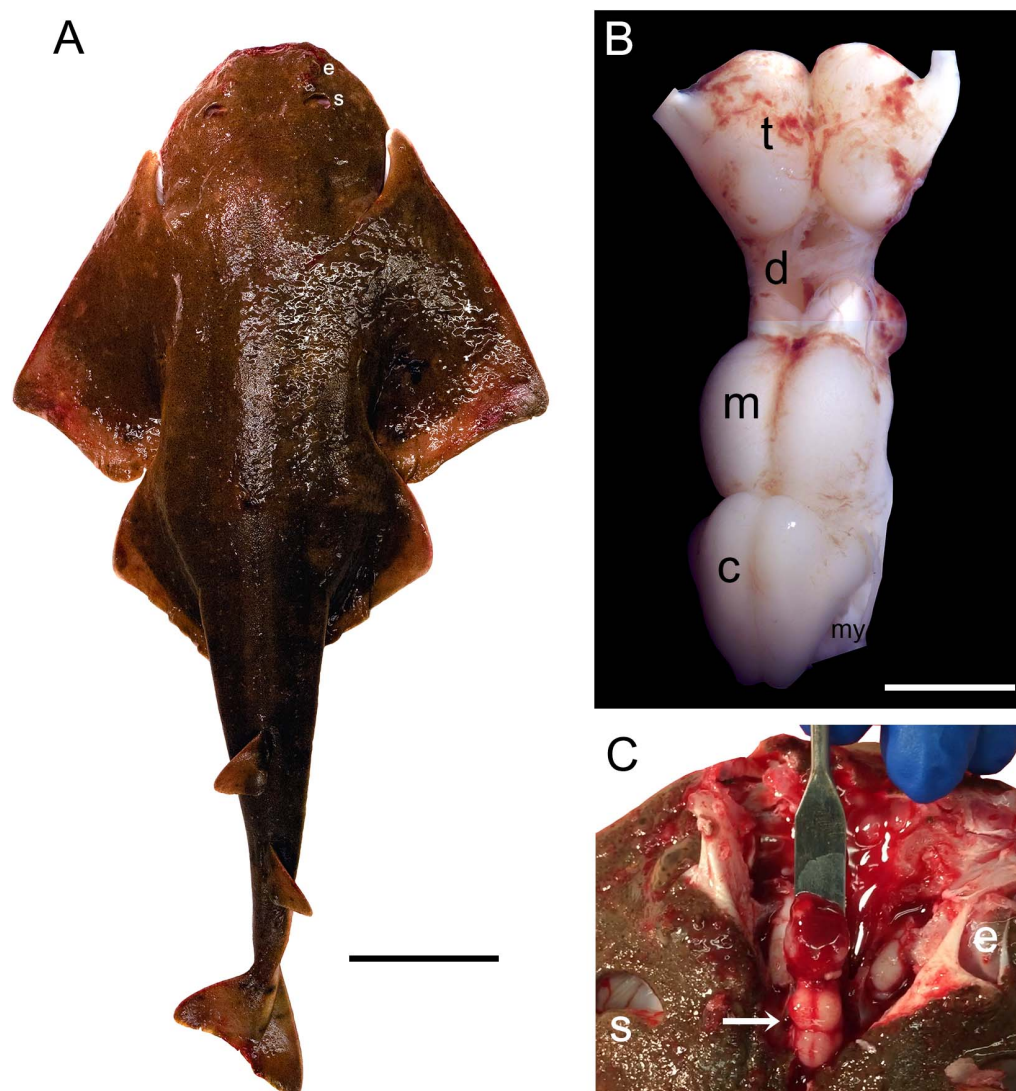
FIGURE 1

(A) The Pacific angelshark (a female specimen). Scale bar = 10 cm. (B) The Pacific angelshark brain [t, telencephalon; d, diencephalon; m, mesencephalon; c, cerebellum; my, myelencephalon (ventral to the cerebellum, only partially visible)]. The olfactory bulbs have been removed. Scale bar = 5 mm. (C) The Pacific angelshark brain (arrow) *in situ*. e, eye; s, spiracle.

corresponded to the mesencephalic trigeminal nucleus described in other shark species (Roberts and Witkovsky, 1975; Witkovsky and Roberts, 1975, 1976; MacDonnell, 1980, 1983, 1984, 1989). Consistent with these observations, the angelshark cells had thick subependymal processes, and some of their somata penetrated the ependyma to come into direct contact with the cerebrospinal fluid (CSF; Figures 3E, F). Somata inside the ependymal layer were consistently observed across the specimens, suggesting it was not a sectioning artifact.
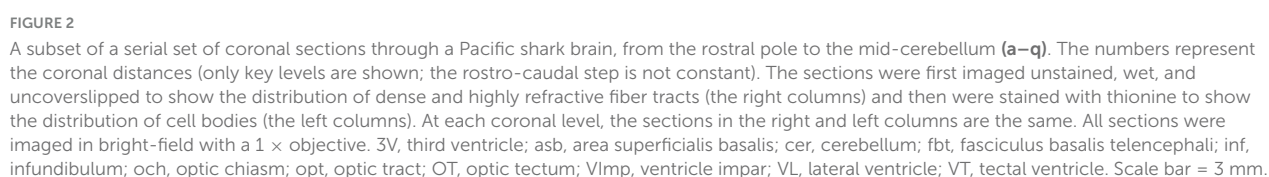
The angelshark cerebellum had a structure typical for elasmobranchs (Figures 3G, H). The granule cells were concentrated in the granular eminences (Butler and Hodos, 2005), long rostro-caudal columns that appeared nearly circular in some coronal sections.

We have previously shown that the ependymoglia of at least some galeomorph sharks shows strong immunoreactivity for ionized calcium-binding adapter molecule 1 (Iba1, AIF-1), a protein that is associated with immune responses and that is also a specific marker for the microglia in mammalian brains (Janušonis, 2018). Iba1 was also strongly expressed in the ependymoglia of the angelshark telencephalon (Figure 4A), with ependymoglial processes often covering capillaries (Figures 4B, C). Strong Iba1-immunoreactivity was also present in more caudal regions (Figures 4D, E).

3.2 The anatomical organization of forebrain serotonergic fibers

Consistent with the general vertebrate pattern, a major source of serotonergic fibers in the angelshark brain is the brainstem raphe nuclei. Many of these fibers originate in the midbrain tegmentum (Figure 5A) and spread through neural tissue. In addition, a
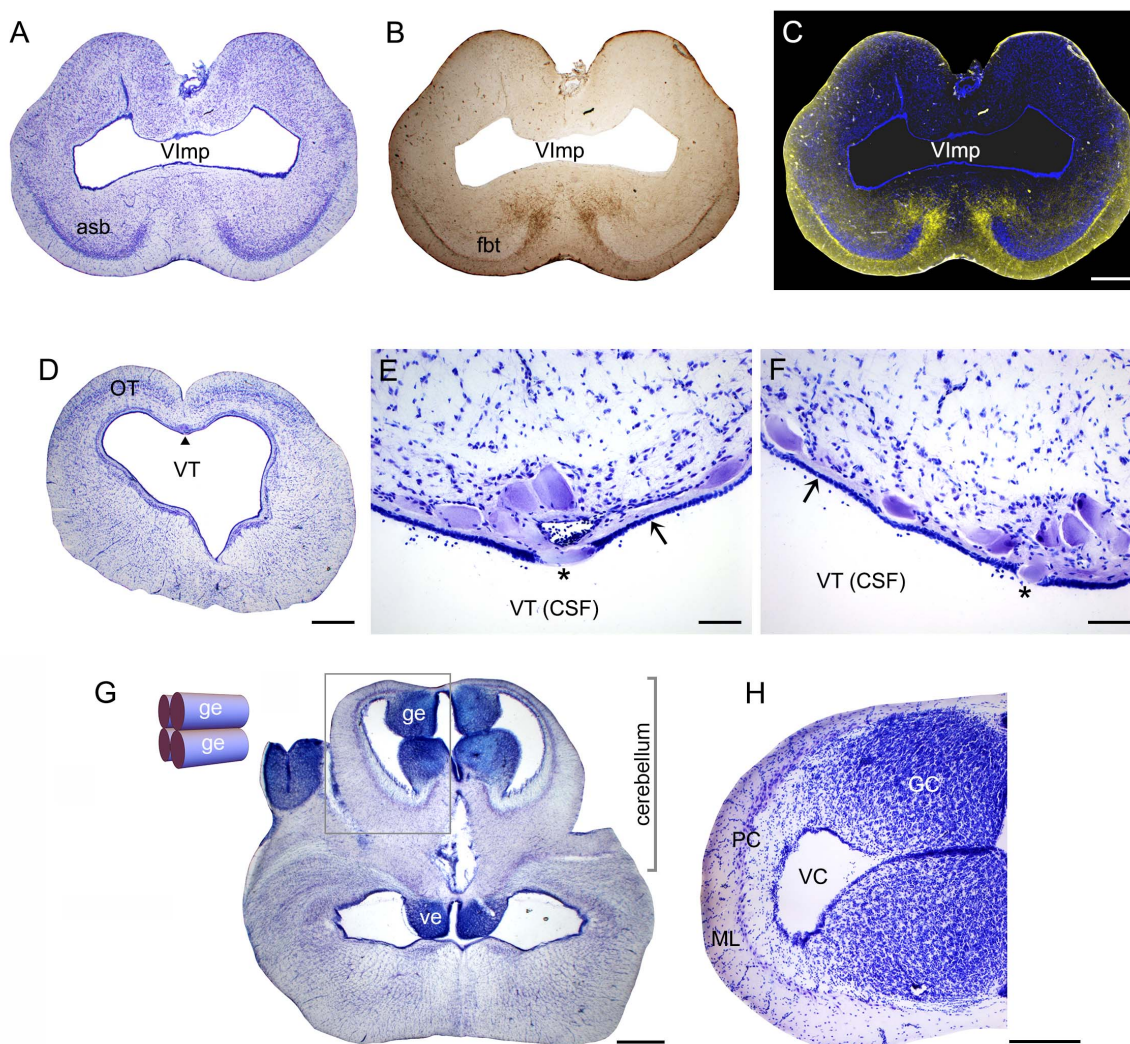
FIGURE 2
A subset of a serial set of coronal sections through a Pacific shark brain, from the rostral pole to the mid-cerebellum **(a–q)**. The numbers represent the coronal distances (only key levels are shown; the rostro-caudal step is not constant). The sections were first imaged unstained, wet, and uncoverslipped to show the distribution of dense and highly refractive fiber tracts (the right columns) and then were stained with thionine to show the distribution of cell bodies (the left columns). At each coronal level, the sections in the right and left columns are the same. All sections were imaged in bright-field with a 1 × objective. 3V, third ventricle; asb, area superficialis basalis; cer, cerebellum; fbt, fasciculus basalis telencephali; inf, infundibulum; och, optic chiasm; opt, optic tract; OT, optic tectum; VImp, ventricle impar; VL, lateral ventricle; VT, tectal ventricle. Scale bar = 3 mm.

FIGURE 3

(A) A coronal section through the telencephalon stained to visualize cell bodies. **(B)** The same section before staining imaged wet to visualize major fiber tracts. **(C)** The two images superimposed (pseudocolored blue and yellow, respectively). **(D)** A coronal section through the mesencephalon stained to visualize cell bodies. The arrowhead indicates the mesencephalic trigeminal nucleus (Me5). **(E,F)** High-power images of Me5, showing thick subependymal processes (arrows) and cell bodies that cross the ependymal layer and come into direct contact with CSF (asterisks). **(G)** A coronal section through the cerebellum and myelencephalon stained to visualize cell bodies. The inset shows a schematic rostro-caudal view of the four granular eminences. **(H)** A high-power image of the cerebellum (approximately corresponding to the boxed area in G). The sections correspond to the following coronal levels in Figure 2: **(A–C)** to level (h), **(D–F)** to level (p), and **(G–H)** to level (q). Sections **(A,D–H)** were stained with thionine; all sections were imaged in bright-field. asb, area superficialis basalis; CSF, cerebrospinal fluid; GC, granule cells; ge, granular eminence; fbt, fasciculus basalis telencephali; ML, molecular layer; OT, optic tectum; PC, Purkinje cells; VC, cerebellar ventricle; ve, ventral eminence; VImp, ventricle impar; VT, tectal ventricle. Scale bars = 1 mm **(A–D,G)**, 100 μm **(E,F)**, 400 μm **(H)**.

major group of serotonin-immunoreactive cells was present in the angelshark hypothalamus (Figure 5B). These cells appeared to make a major contribution to the forebrain serotonergic projections.

The major serotonergic pathways in the forebrain were readily identifiable with 5-HT immunohistochemistry, revealing a relatively complex picture of transitions in the caudo-rostral axis (Figures 5B–H). However, this sequence could be explained by a dynamic interplay of only two driving factors: (*i*) a tendency of fibers to accumulate at tissue borders and (*ii*) an attracting force generated by the dorsal pallium (Figure 5K). This parsimonious approach facilitates the following description of the key pathways, but further confirmatory research is required.

In the diencephalon, many fibers emerged from strongly serotonin-immunoreactive cells that surrounded the ventricle in the inferior lobe of the hypothalamus (a large structure in shark brains). In this ventral region, fibers tended to accumulate at high densities near the ventricular and pial surfaces, with no identifiable orientation (Figures 5B, 6A). In the dorsal region at the same coronal level, fibers formed a distinct oriented stream that coursed in the dorsal direction and then made a lateral turn to approach the habenula (Figures 6A, B). Some of these fibers appeared to emerge from an initially disorganized cluster of fibers located midway between the ventral and dorsal regions (Figure 6C). The fiber stream entered the habenula at the initial approach angle, but some fibers appeared to
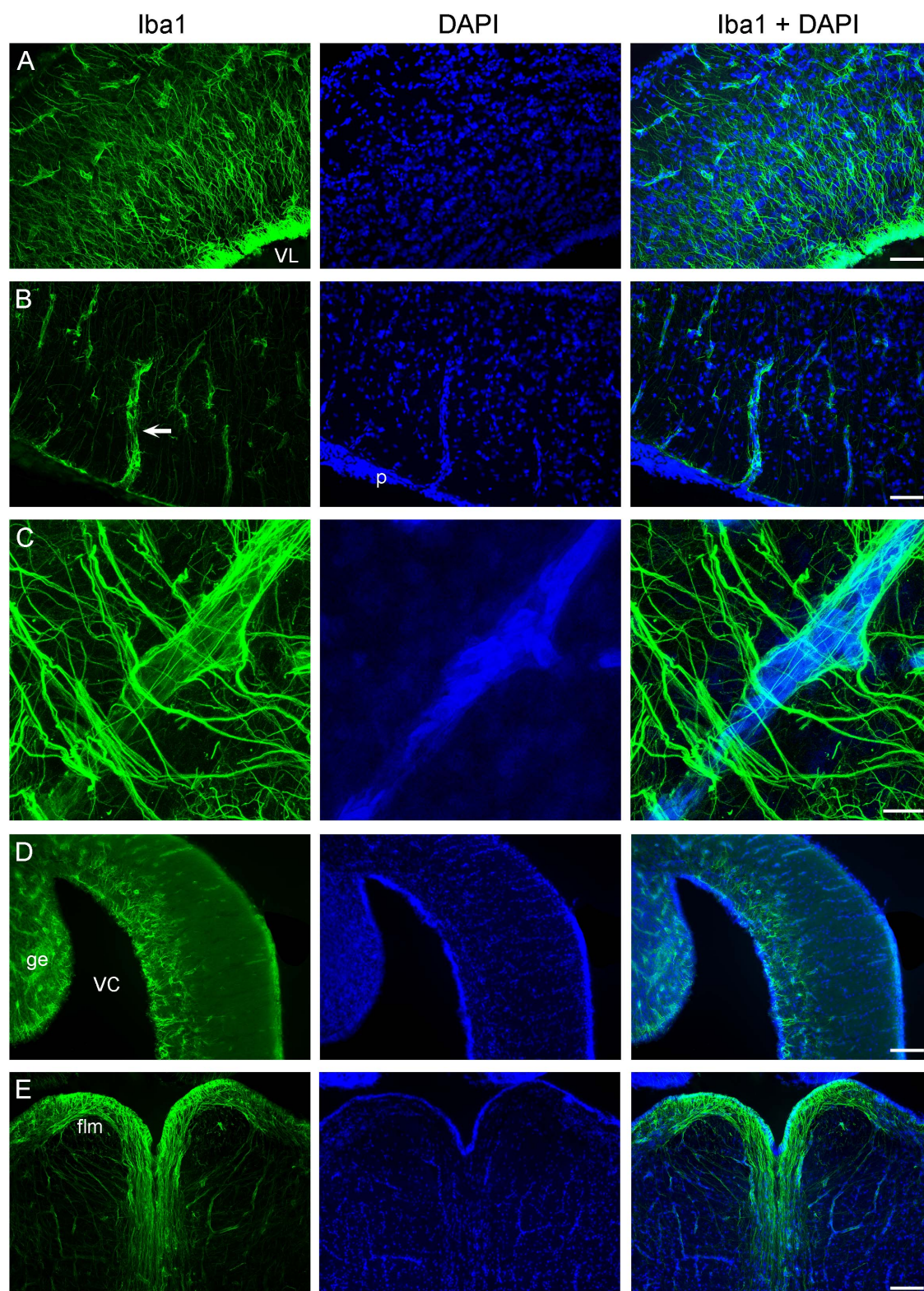
FIGURE 4
Iba1-immunoreactivity in the brain (cell nuclei are visualized with DAPI). **(A)** An epifluorescence image of Iba1+ ependymoglial cells in the telencephalon. The cell bodies are located at the lateral ventricle (VL) and extend their processes into brain parenchyma. **(B)** An epifluorescence image of a blood vessel (arrow) in the telencephalon. The blood vessel enters brain parenchyma through the pia (p) and is surrounded by Iba1+ processes. **(C)** A confocal image of a blood vessel in the telencephalon, with many fasciculated Iba1+ processes. The image is a maximum-intensity projection of 71 optical sections. **(D)** An epifluorescence image of Iba1-immunoreactivity in the cerebellum, at approximately the same coronal level as Figure 3G (ge, granular eminence; VC, cerebellar ventricle). **(E)** An epifluorescence image of Iba1+ fibers in the myelencephalon, at approximately the same coronal level as Figure 3G (flm, fasciculus longitudinalis medialis). Scale bars = 100 μm **(A,B)**, 25 μm **(C)**, 200 μm **(D,E)**.
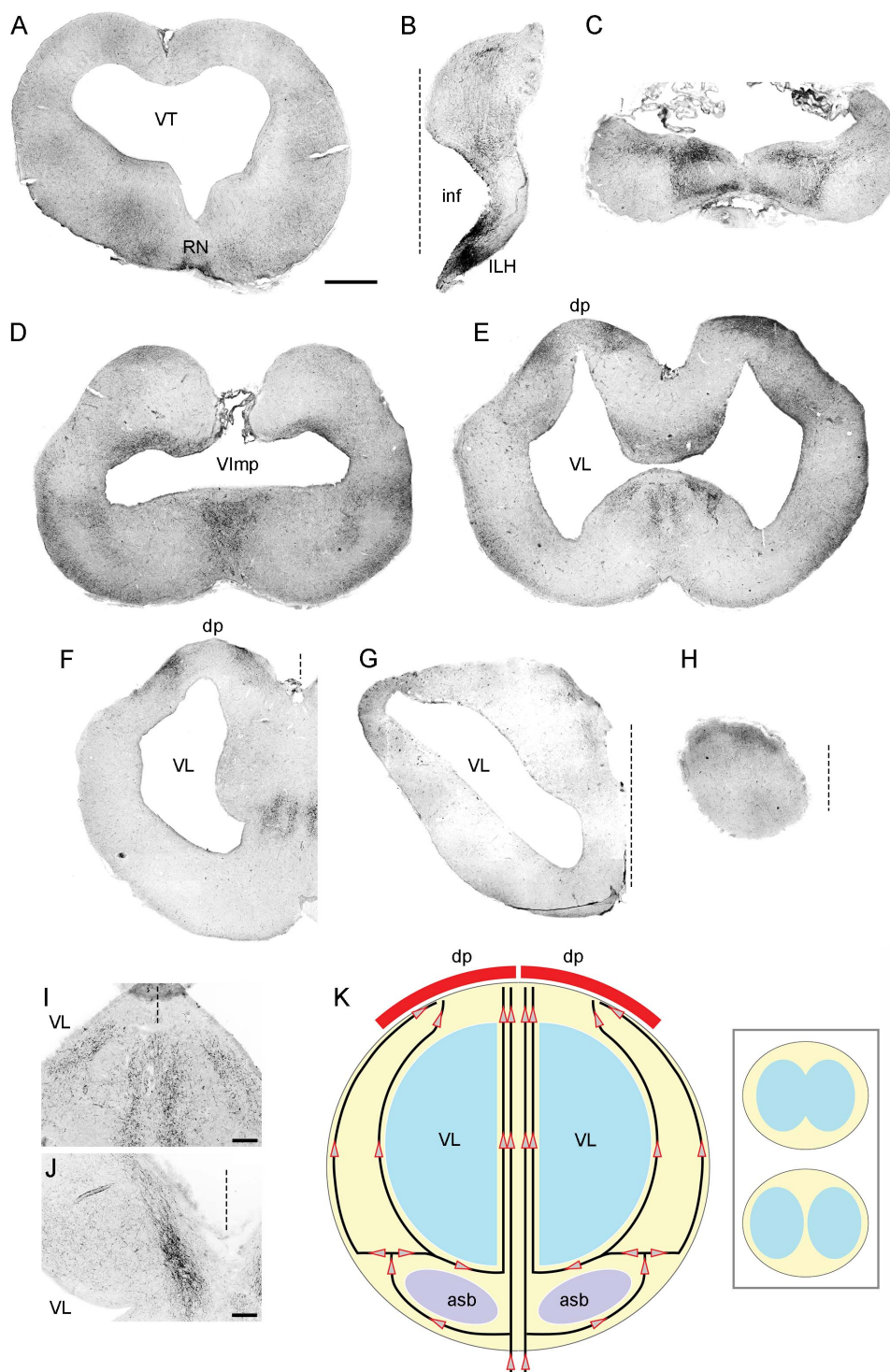
FIGURE 5
(A−H) Epifluorescence images of 5-HT-immunoreactivity at 8 coronal brain levels. Each image is a montage composed of 4−32 images captured with a 5 × objective. The montages were converted to grayscale and digitally inverted (higher densities of serotonergic fibers are darker). The original montages (at full resolution and in color) are available in the Supplementary material. **(I)** A higher-power image of 5-HT-immunoreactivity in a region corresponding to the ventromedial region of **(E)**. Four streams of serotonergic fibers are apparent. **(J)** A higher-power image of 5-HT-immunoreactivity in a region corresponding to the dorsomedial region of **(G)**. A medial stream of serotonergic fibers entering the dorsal pallium is apparent. **(K)** The hypothesized paths of serotonergic fibers. The key observations in **(A−J)** can be explained by assuming that the forebrain serotonergic fibers tend to accumulate close to pial and ependymal surfaces (perhaps due to their intrinsic stochasticity) but are additionally pulled by a deterministic force exerted by the dorsal pallium (dp). The inset schematically shows the emergence of the median tissue bridge (the top configuration is caudal to the bottom one; they approximately correspond to panels **(E)** and **(F)**, respectively). asb, area superficialis basalis; dp, dorsal pallium; ILH, inferior lobe of the hypothalamus; inf, infundibulum; RN, raphe nuclei; VImp, ventricle impar; VT, tectal ventricle. The midline is indicated by dashed lines. Scale bars = 1 mm **(A−H)**, 200 μm **(I,J)**.
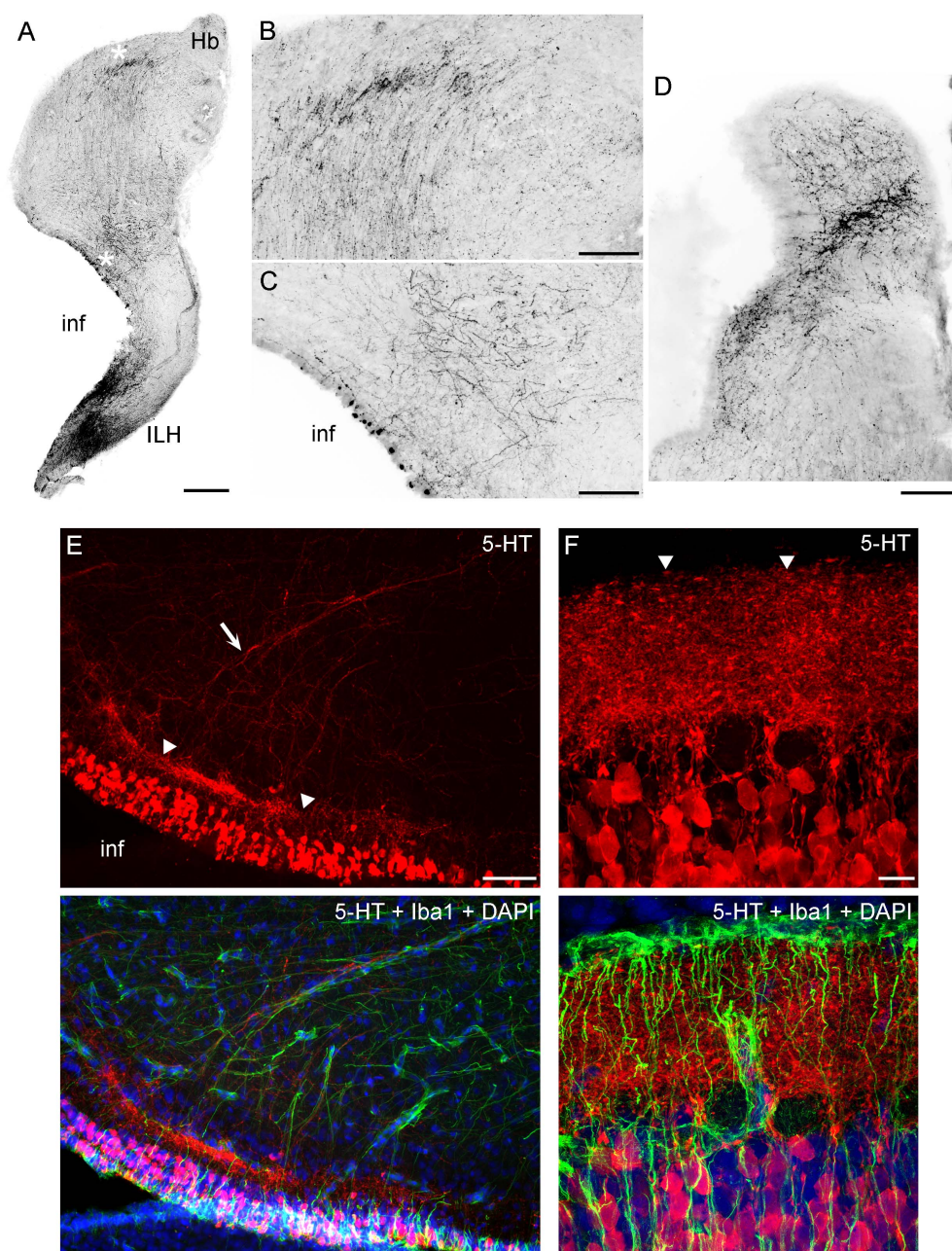
FIGURE 6
(A–D) Epifluorescence images of 5-HT immunoreactivity in coronal sections through the diencephalon. The images were converted to grayscale and digitally inverted (higher densities of serotonergic fibers are darker). **(A)** An image of one side of the diencephalon (corresponding to Figure 5B). **(B,C)** Two enlarged regions of **(A)** (marked with asterisks). In **(B)**, note the strongly oriented fibers coursing toward the habenula. **(D)** A stream of fibers in the habenula, at a coronal level adjacent to that of (A). **(E)** An epifluorescence image of the hypothalamus immunostained for 5-HT and Iba1 (with DAPI to visualize nuclei). **(F)** A confocal image of the caudal hypothalamus immunostained for 5-HT and Iba1 (with DAPI to visualize nuclei). The image is a maximum-intensity projection of 35 optical sections. ILH, inferior lobe of the hypothalamus; inf, infundibulum; Hb, habenula. Scale bars = 500 μm **(A)**, 200 μm **(B–D)**, 100 μm **(E)**, 20 μm **(F)**.

reorient themselves to next proceed to the caudal telencephalon (Figure 6D).

In the caudal telencephalon, fibers again accumulated at the pial and ventricular surfaces, with an additional dorsal pull (Figure 5C). Most fibers moved around the expected location of the fbt (Figure 2 at 5.60 mm), consistent with the poor penetration of dense axon tracts by serotonergic fibers (Janušonis et al., 2020). More rostrally, fibers continued to accumulate near the pial and

ventricular surfaces (Figure 5D). In addition, a medial stream of fibers emerged at the coronal level of the ventricle impar. This stream could be explained by the opening of the median "land-bridge" between the ventral and dorsal parts of the telencephalon (the septal and medial pallial regions). This bridge splits the single ventricle impar (Figure 5D) into the two lateral ventricles more rostrally (Figures 5E, F) and can serve as a shortcut between the ventromedial telencephalon and the dorsal pallium. Consistent

with this possibility, fibers formed four distinct medial streams, two on each side (Figure 5F). Of the two streams, the more lateral one approached the bridge as a continuation of the fibers that spread near the ventricle (Figures 5E, I). The other stream, adjacent to the median symmetry line, appeared to contain fibers that initially accumulated near the ventral pial surface but then were pulled in the dorsal direction (toward the medial pallium) when the more direct path to the dorsal telencephalon opened up (Figures 5E, I, K).

In the mid-level telencephalon, two high-density clusters of fibers were present in the dorsal pallium (Figure 5F). These clusters appeared to correspond to (i) fibers that approached the dorsal pallium moving around the ventricles (i.e., taking the longer lateral route), primarily staying close to the pial and ventricular surfaces, and (ii) fibers that used the shorter median route (Figure 5K). The median projection to the dorsal pallium was directly visualized at a more rostral level (Figures 5G, J). The rostral pole of the brain still had a higher accumulation of fibers at the dorsal surface (Figure 5H).

High-resolution imaging of the serotonin-containing cells in the periventricular hypothalamus (Figures 6E–F) suggests a highly organized structure that bears some anatomical resemblance to the serotonin system in the mammalian gut (enterochromaffin cells and serotonergic neurons in the gut wall) (Furness and Stebbing, 2018; Gershon and Margolis, 2021). These cells were uniform in their ovoid morphology (around 20 μm in length) and were densely packed around the ventricle in a continuous layer (around 100 μm thick). At some coronal levels, a distinct, dense serotonin-immunoreactive plexus was present under the cell-body layer, with fiber fascicles emerging from it (Figure 6E). This plexus could be nearly as thick as the cell-body layer and appeared to contain extremely tightly packed neurites whose individual paths could not be distinguished in confocal microscopy at the limit of optical resolution (Figure 6F). The fascicles moved dorsolaterally, entering the described pathway toward the habenula. However, this analysis cannot rule out that some of these fibers were contributed by more caudal regions (e.g., the raphe nuclei).

A systematic analysis of serotonergic fibers at the pial surface of the telencephalon revealed universally elevated densities (Figure 7). Fiber densities showed some regional variation but were consistently higher near the pia with respect to the underlying (deeper) tissue.

The angelshark brainstem poses challenges in computational simulations because it contains many dense axon tracts ("obstacles") (Figure 2); therefore, it was not a focus of this study. Serotonergic fibers in the brainstem are produced by the raphe nuclei that were well developed in the angelshark brain (Figures 8A, B). Notably, serotonergic fibers did not produce a detectable accumulation at the pial and ventricular surfaces of the optic tectum (Figures 8C–F).

3.3 The supercomputing simulation of serotonergic fibers

The described anatomical data were used to build and verify a predictive computational model of serotonergic fiber densities. The model was deliberately minimal in that it consisted only

of FBM trajectories, or idealized fibers, moving unguided within a three-dimensional shape that precisely matched the geometry of the Pacific angelshark brain. Despite its conceptual simplicity, the model was computationally expensive (due to the inherent mathematical properties of FBM) and required supercomputing resources. The hypothesized force toward the dorsal pallium was not included because the current biological information is insufficient to define it quantitatively.

An accurate, three-dimensional model of the Pacific angelshark brain was built based on an anatomical series of sections. The 2D-shapes at each coronal level closely followed the contours of physical sections and were minimally edited to only smooth the contours and achieve a perfect bilateral symmetry (Figure 9). Next, 4800 fibers were launched from the brainstem and were allowed to roam in the brain shape with no internal obstacles. After the fibers achieved stable regional densities (Figure 10), they were compared to those in the biological angelshark brain.

Generally, fibers accumulated near tissue borders, especially at the pial border (Figures 10A–P). This result was highly consistent with the elevated densities of serotonergic fibers at the pial border of the angelshark telencephalon (Figure 7). In the diencephalon, a dense accumulation of simulated fibers was observed in the region surrounding the ventricle in the inferior lobe of the hypothalamus (Figures 10D–F, Q). This pattern was similar to the elevated densities of serotonergic fibers in this region of the biological brain (Figure 6A). The simulated densities were also high at the pial surface of the dorsal lobes overhanging the ventricle impar of the telencephalon (Figures 10H, R), as well as in the prominent bulges of the dorsal pallium (Figures 10K, S). This pattern was again consistent with the serotonergic fiber densities in the biological brain (Figures 5D, E). Increased simulated and biological densities were present in the rostral dorsolateral telencephalon near the attachment of the stalk of the olfactory bulbs (Figures 5G, 10M, N, T). The biological and simulated density values showed good correspondence along cuts that traversed entire sections (Figure 11).

4 Discussion

4.1 General neuroanatomical observations

The gross morphology and basic cytoarchitecture of the Pacific angelshark brain share strong similarity with those of the spiny dogfish (*Squalus acanthias*), another squalomorph shark in a different (Squaliformes) order (Smeets et al., 1983; Smeets, 1998; Butler and Hodos, 2005). Compared to other sharks, where the cerebellar structures can make up over 40% of the brain (New, 2001; Montgomery et al., 2012), the angelshark cerebellum is small, probably because this species is a sedentary, ambush predator. A comprehensive rostro-caudal set of coronal sections was produced in this study (Figure 2; Data availability statement), but we primarily focused on the brain geometry and the physical distribution of cell bodies (important for the modeling of serotonergic fibers). We did not investigate deeper levels of neural tissue organization that would require chemoarchitectonic or tract-tracing analyses (Smeets, 1998; Paxinos et al., 2022).
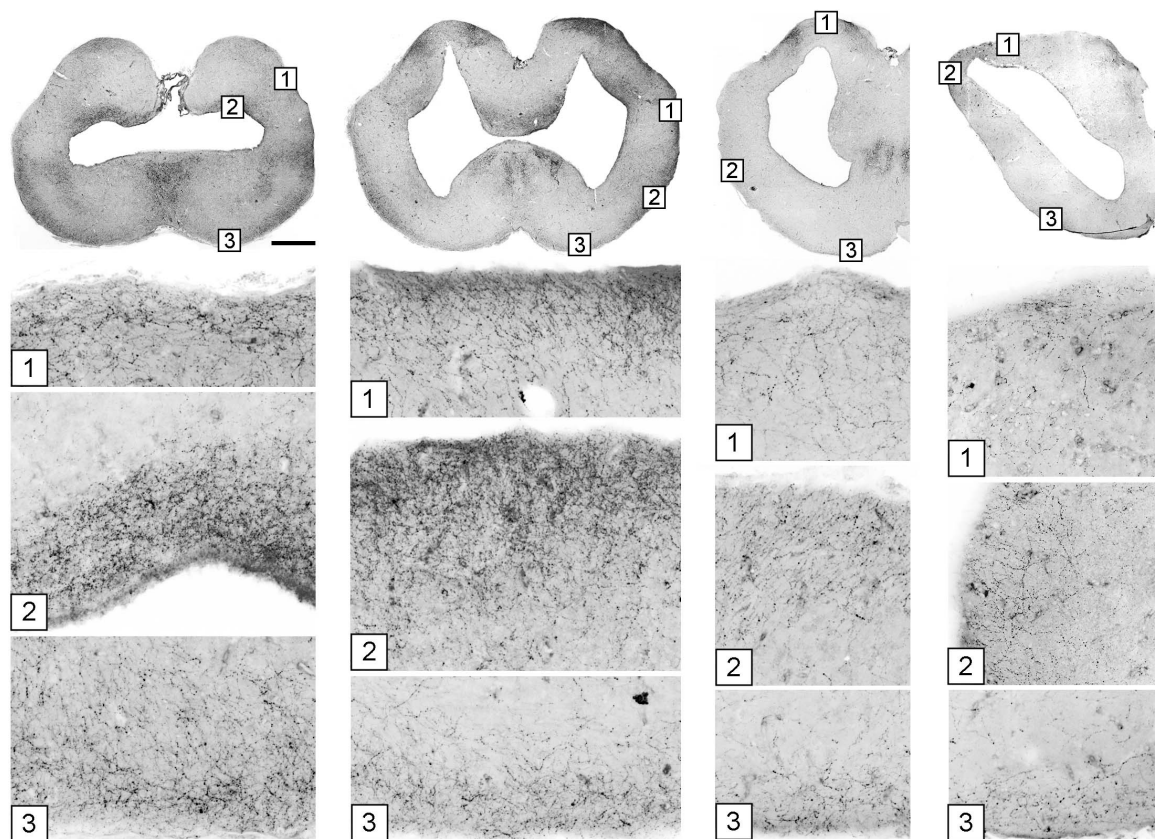
FIGURE 7
The accumulation of serotonergic fibers near tissue borders in the forebrain. The images in the top row correspond to Figures 5D–G. Under each coronal level, the high-power images show the accumulation of 5-HT+ fibers in border regions marked with corresponding numbers. The sections were immunostained for 5-HT, imaged in epifluorescence, converted to grayscale, and digitally inverted (higher densities of serotonergic fibers are darker). Some high-power images are rotated to orient the edge horizontally. Scale bars = 1 mm (top row), 100 μm (all panels below).

Specifically, regions that appear homogeneous in the overall distribution of cells may contain well-defined subregions that are distinctly different in their functional network profiles (e.g., neurotransmitters, receptors, projections). With these limitations, this study contributes to comparative neuroanatomy, including two notable observations.

First, strong Iba1-immunoreactivity was observed in the ependymoglial (and potentially other) cells in the angelshark brain. This finding extends our previous report (Janušonis, 2018) and leads to the conclusion that, generally, Iba1 is expressed in the brains of both squalomorph and galeomorph sharks. However, it may not be expressed in some shark branches that diverged early (Janušonis, 2018). It is unknown whether the detected molecule is analogous to the mammalian Iba1, expressed in microglia (Wake et al., 2009), or is a functionally different molecule with a strong structural similarity to Iba1. Extensive research has shown that Iba1, also known as AIF-1, is highly conserved across the animal kingdom (Barca et al., 2017).

Second, a prominent mesencephalic trigeminal nucleus (Me5) was found in the angelshark brain. This nucleus, located on the midline in the roof of the tectal ventricle, contains gigantic cells (measuring 50–100 μm across) with thick processes that extend laterally just below the ependyma. Some cell bodies protrude ventrally into the ventricle and appear to reach the CSF. This remarkable arrangement was studied in other shark species in a series of publications in the 1980s (MacDonnell, 1980, 1983, 1984, 1989), which followed earlier light microscopy, electron microcopy, and electrophysiological studies (Roberts and Witkovsky, 1975; Witkovsky and Roberts, 1975, 1976). Me5 is interesting because it is the only primary sensory ganglion located within the CNS (Witkovsky and Roberts, 1975; Blumenfeld, 2022) and because of its role in clinical neurology (Blumenfeld, 2022). In the human brain, Me5 neurons form two lateral clusters and are known to mediate the monosynaptic jaw-jerk reflex. This reflex may be undetectable in healthy individuals but may become unmasked in conditions such as amyotrophic lateral sclerosis (ALS; Blumenfeld, 2022). A detailed electrophysiological study has described a similar reflex in the smallspotted catshark (*Scyliorhinus canicula*) and the dusky smoothhound (*Mustelus canis*) (galeomorph sharks, also known as dogfish), which suggests that this fast jaw-closing mechanism has been conserved in vertebrates (Roberts and Witkovsky, 1975). Our analysis supports an earlier hypothesis that, in sharks, Me5 activity (and the associated jaw closing) can be directly modulated by signals in the CSF (MacDonnell, 1980). This connection may have been lost in the reptiles and mammals, where Me5 is no longer adjacent to the ventricular wall (MacDonnell, 1980). We lastly note that the size of the Me5 neurons in the angelshark may be related
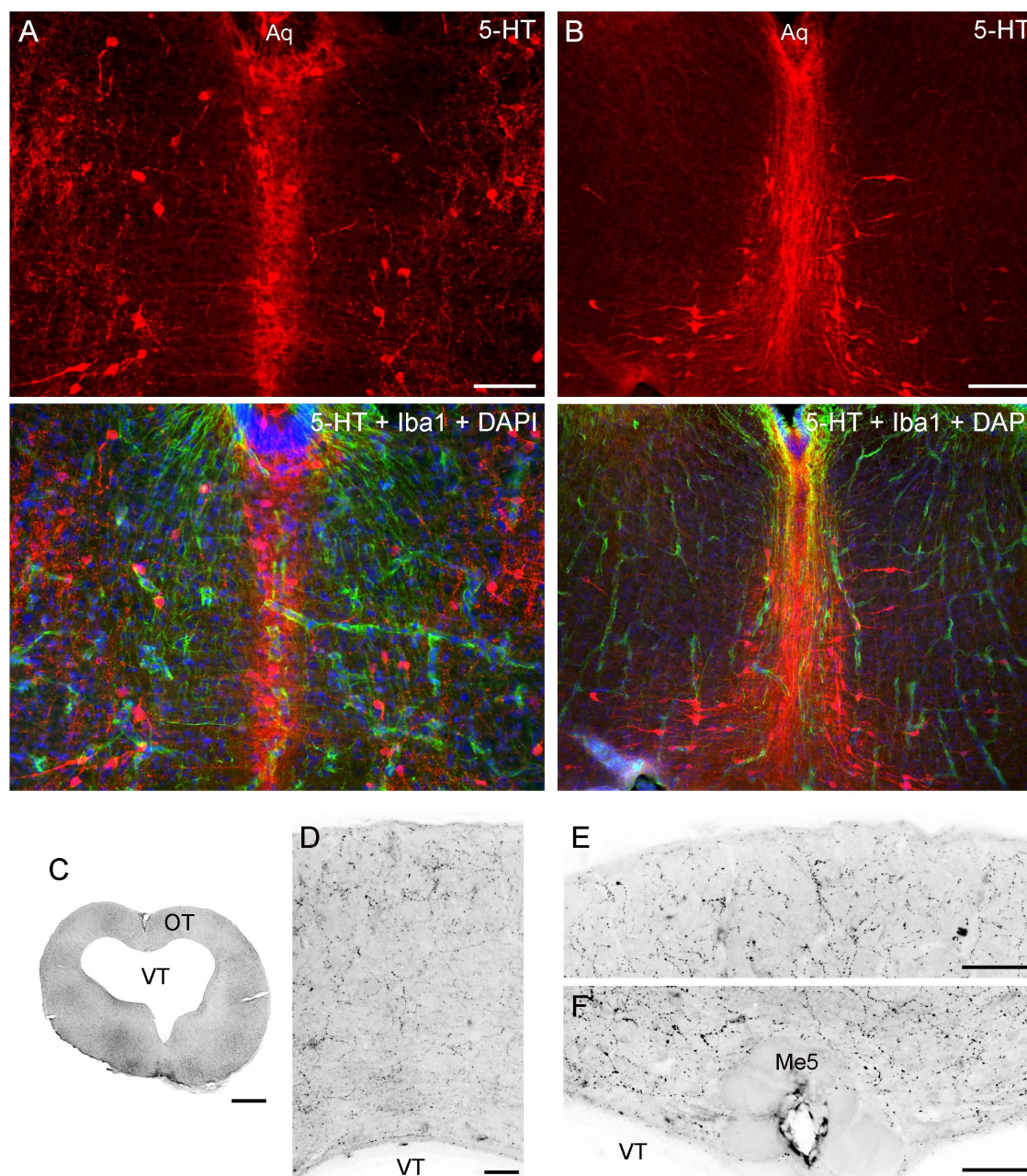
FIGURE 8

(A,B) Epifluorescence images of the raphe nuclei in coronal sections through the tegmentum stained for 5-HT and Iba1 (with DAPI to visualize nuclei). **(C–F)** Epifluorescence images of 5-HT immunoreactivity in coronal sections through the mesencephalon. The images were converted to grayscale and digitally inverted (higher densities of serotonergic fibers are darker). **(C)** An entire section corresponding to Figure 5A. **(D)** An enlarged image of the optic tectum (OT). **(E)** A high-power image of the superficial OT. **(F)** A high-power image of the periventricular OT. Aq, aqueduct; Me5, mesencephalic trigeminal nucleus; VT, tectal ventricle. Scale bars = 100 μm (A, D-F), 200 μm (B), 1 mm (C).

to its powerful, extensible jaws that snap upward to capture prey within the striking distance of the immobile, camouflaged animal.

The angelshark telencephalon is relatively uniform in its spatial distribution of cell bodies (with the exception of the asb) and is virtually devoid of large-scale "obstacles" in the form of major axon tracts (with the exception of the fbt). It makes it a convenient natural model for large-scale simulations of serotonergic fibers. By comparison, a number of major axon tracts are present in all divisions of the adult mammalian brain, including the telencephalon (e.g., the anterior commissure, the corpus callosum).

These tracts can be impenetrable to serotonergic fibers to various degrees (Lidov and Molliver, 1982; Janušonis et al., 2020). Mouse telencephalic regions also show differences in viscoelasticity, which are only partially understood (Antonovaite et al., 2021).

Compared to the telencephalon, the angelshark brainstem is highly refractive, likely due to densely packed axon tracts (Smeets, 1998). This observation is supported by viscoelastic measurements in the zebrafish (*Danio rerio*) brain that show that fish telencephalon is more viscous than the brainstem (which is stiffer) (Jordan et al., 2022). In the brainstem, axon tracts are
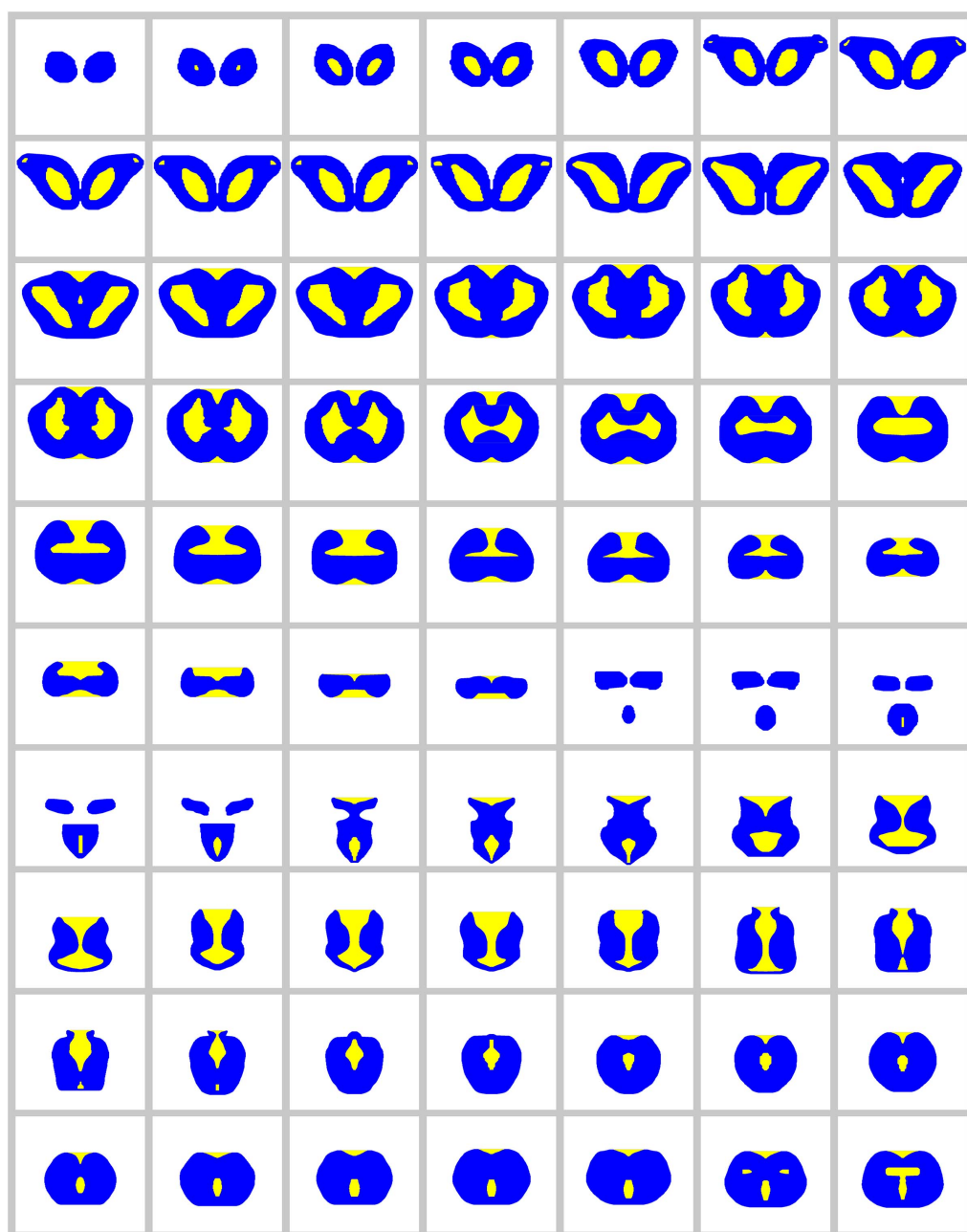
FIGURE 9
The complete series of digitized, bilaterally symmetrized contours used to build the 3D-model of the angelshark brain for simulations (blue, permissive regions; yellow, forbidden regions).

expected to have different orientations and introduce strong local anisotropies. The current experimental data is insufficient to model these anisotropies accurately.

4.2 Serotonergic fiber paths: from comparative neuroanatomy to predictive modeling

The primary sources of serotonergic fibers in the angelshark brain are the raphe nuclei of the brainstem and the inferior lobe of the hypothalamus. Raphe clusters of serotonergic neurons are a universal vertebrate feature (Jacobs and Azmitia, 1992; Stuesse et al., 1995; Hornung, 2003; Rodrigues et al., 2008; Lillesaar, 2011; Fonseca et al., 2021). Serotonergic hypothalamic neurons have been reported in other shark species, with additional clusters in other brain regions, such as the preoptic area, the pretectal area, and the habenula (Stuesse et al., 1991; Carrera et al., 2008; Lillesaar, 2011). However, serotonin immunoreactivity in these additional regions may be developmentally transient (Carrera et al., 2008), consistent with similar observations in the development of bony fishes (Ebbesson et al., 1992). Hypothalamic serotonergic
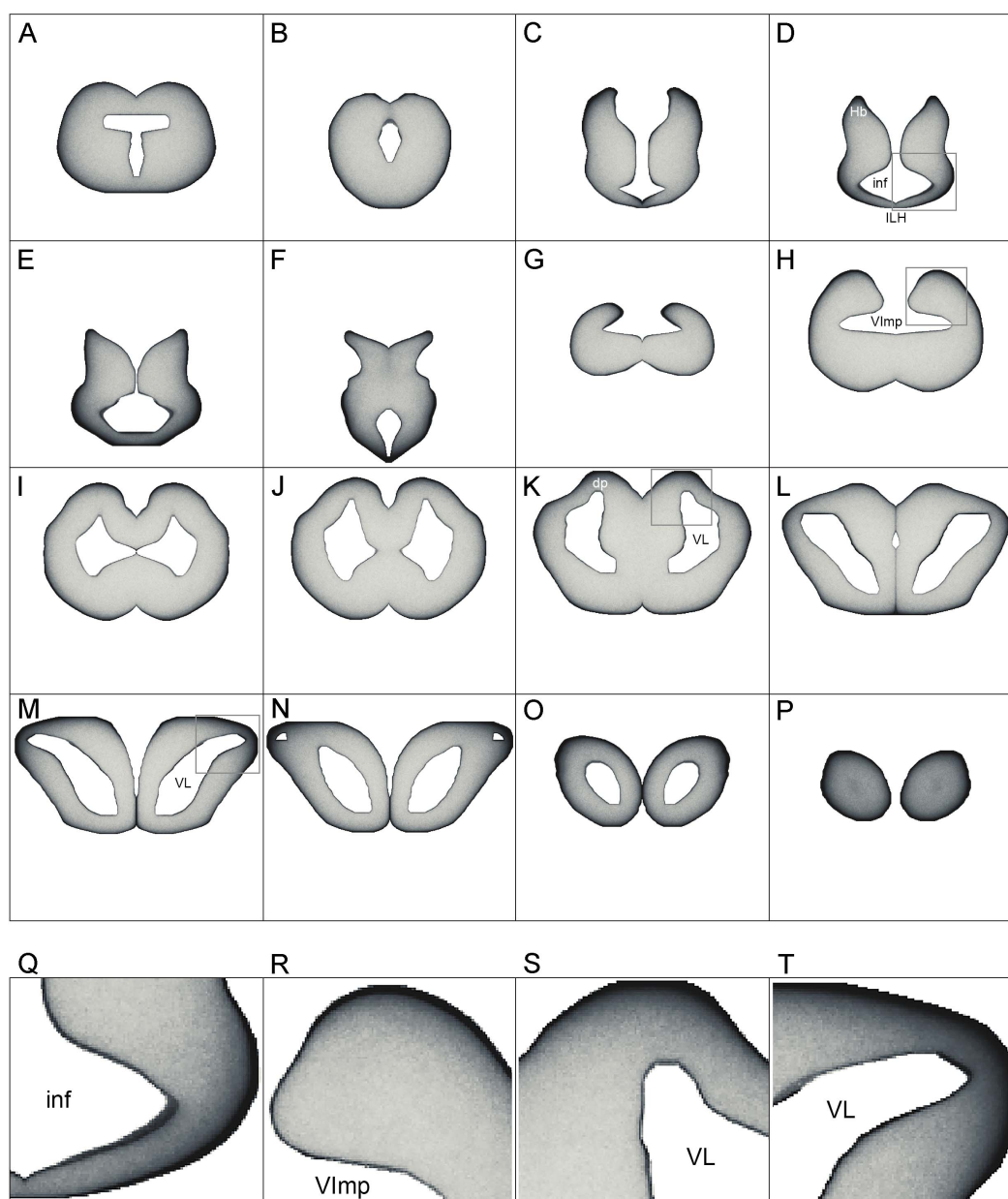
FIGURE 10
(A–P) The simulated densities of serotonergic fibers modeled as stochastic paths of fractional Brownian motion (FBM). Key coronal levels are shown. In the simulation, the fibers receive no guiding cues; regional density differences are the result of the brain geometry and the fundamental properties of FBM. Higher densities are darker, to facilitate comparisons with Figure 5. The images have no artificial contour lines (borders appear black because of fiber accumulation). (Q–T) Enlarged regions of (D), (H), (K), and (M), respectively (boxed). dp, dorsal pallium; ILH, inferior lobe of the hypothalamus; inf, infundibulum; Hb, habenula; VImp, ventricle impar; VL, lateral ventricle.

neurons also have been reported in reptiles, but not consistently across species (Rodrigues et al., 2008). They appear to have been lost in mammals, with the only but remarkable exception of the monotremes (egg-laying mammals) (Manger et al., 2002).

Both raphe and hypothalamic neurons may contribute serotonergic fibers to the telencephalon. A developmental study of the smallspotted catshark has shown the presence of pioneering fibers in the telencephalon after the differentiation of the raphe serotonergic neurons but just before the sudden ("explosive") appearance of the hypothalamic serotonergic neurons (Carrera et al., 2008). In the angelshark, hypothalamic serotonergic cells

are densely packed at the infundibular ependymal layer (in the inferior lobe of the hypothalamus) and appear to give rise to a number of laterally-projecting fascicles. Hypothalamic and raphe fibers can potentially interact in the distinct plexus overlying some hypothalamic serotonergic cells (Figures 6E, F) or in more lateral fiber clusters that in coronal sections appear disorganized (Figure 6C) but may give rise to highly oriented fibers directed toward the habenula (Figure 6B). In mammals, raphe fibers also enter the hypothalamus; in embryonic rat development, serotonergic axons that reach the infundibular recess (the primordial mammillary complex) are among the first
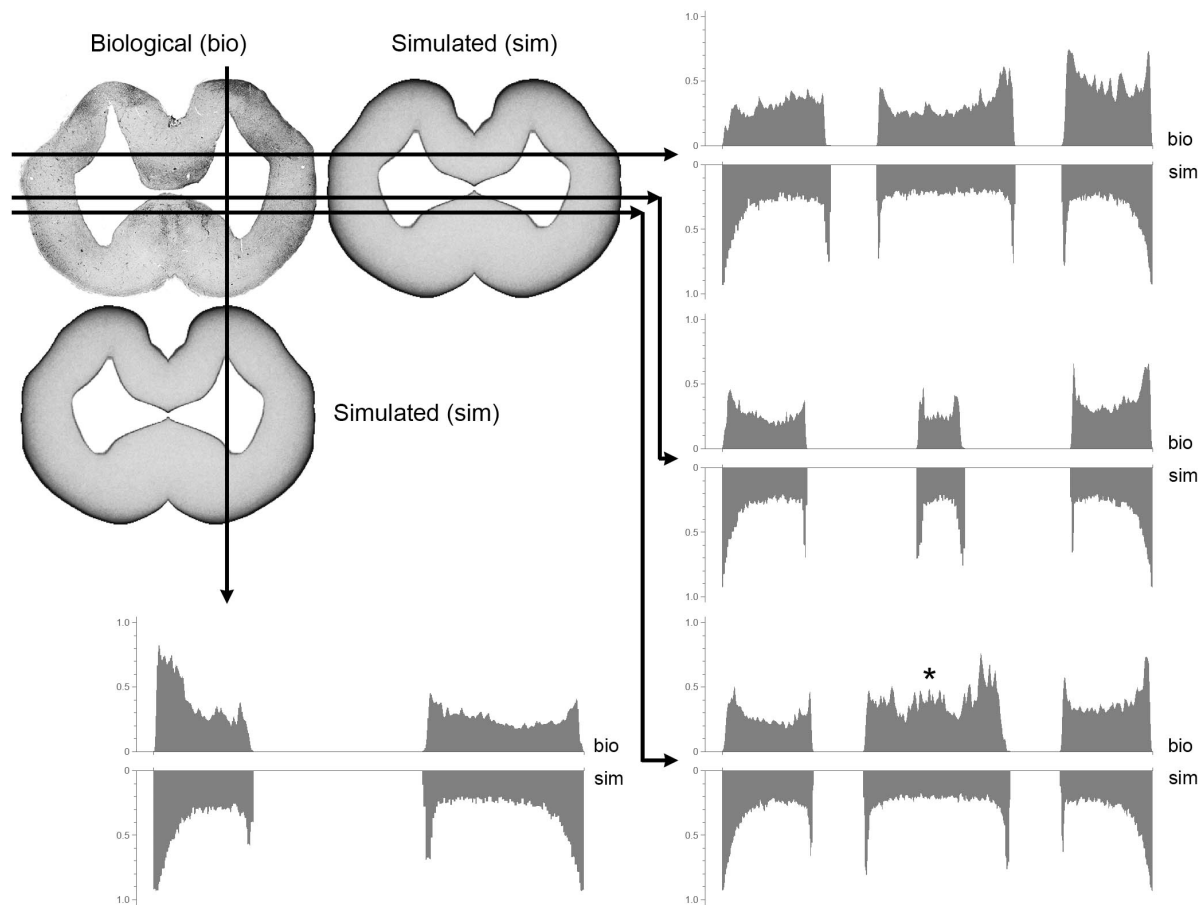
FIGURE 11
A comparison between biological (visualized with immunohistochemistry; bio) and simulated (sim) fiber densities at a mid-telencephalic level (Figure 5E). The grayscale pixel values (intensities) along each of the four cuts are shown in graph pairs. In each pair, the top and bottom graphs read out the biological and simulated values, respectively (left-to-right, following the direction shown by the arrows). All Y-axes range from 0 (white) to 1 (black) and point upward or downward for the biological or simulated values, respectively. A good match is indicated by a mirror-symmetry of the plots. The asterisk indicates a significant mismatch produced by medially-located fibers pulled toward the dorsal pallium (such deterministic forces were not included in the model).

serotonergic fibers to arrive in the forebrain (Lidov and Molliver, 1982; Jacobs and Azmitia, 1992). There are no hypothalamic serotonergic neurons in the rat brain, but comingling between raphe and hypothalamic serotonergic fibers has been shown in monotremes (Manger et al., 2002). Since both raphe and hypothalamic serotonergic neurons are anatomically associated with the ventricular system, one of their original functions may have been to convey CSF-related information to neural tissue (Parent, 1981), thus supporting global functional integration of the CNS.

The observed distribution of serotonergic fibers in the telencephalon allows for a parsimonious description, based on a framework introduced in our recent publications (Janušonis et al., 2020; Janušonis et al., 2023; Mays et al., 2023). Specifically, we assume that serotonergic fibers can be guided by a small set of deterministic cues but are inherently stochastic in their trajectories.

In the telencephalon, the *deterministic* component can be well captured by the single observation that serotonergic fibers tend to move toward the dorsal pallium (Figure 5K). The dorsal pallium is an intriguing region in that it may have been absent from the ancestral vertebrate brain and may have emerged several times in different vertebrate lineages, optionally and independently (Striedter and Northcutt, 2020). In particular, in may not be present in amphibians and lungfishes (Striedter and Northcutt, 2020). This hypothesis is consistent with the dual-origin hypothesis of the primate cerebral cortex, a derived dorsal pallial structure with medial and lateral pallial moieties (Pandya et al., 2015). Notably, four distinct fascicles (bands) of serotonergic fibers are present in the angelshark septum (Figures 5F, I), likely *en route* to the medial side of the dorsal pallium. Such fascicles are also prominent in rodents but there they enter the developing cerebral cortex (the cortical plate) (Lidov and Molliver, 1982; Wallace and Lauder, 1983; Vertes, 1991; Vertes et al., 1999). It suggests that these fascicles, and perhaps the two distinct serotonergic bands that initially "sandwich" the mammalian cortical plate (Wallace and Lauder, 1983; Voigt and de Lima, 1991), are not cortex-specific. In fact, the superficial cortical band, which enters the mammalian cortical marginal zone (Janušonis et al., 2004), has a direct counterpart in the angelshark dorsal pallium (Figure 5J). We note that the parsimony of this explanation does not rule out the possibility that other regions, such as the habenula, may also attract serotonergic fibers (Figures 6A, B, D), thus providing additional guidance before
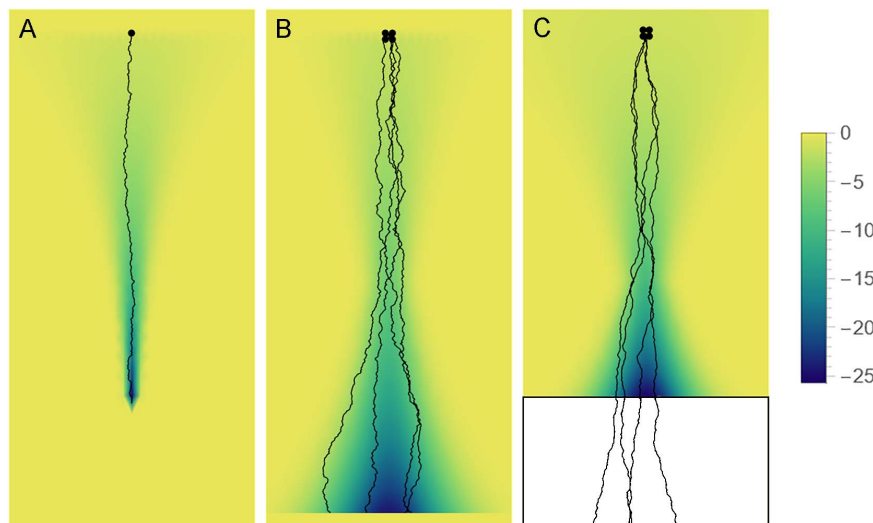
FIGURE 12
Axon paths may be fundamentally stochastic but can be constrained by "effective potential" landscapes (e.g., axon guiding gradients), depending on the axon type. The colors represent the value of the potential (high = yellow, low = blue). **(A)** Some axons may become trapped in a narrowing potential trough and thus be precisely guided to targets (e.g., retinogeniculate axons). **(B)** Some axons may be constrained to more spacious valleys, where their stochasticity may be more apparent (e.g., retinohypothalamic axons). **(C)** Some axons may be guided to specific brain regions in development, to facilitate their dispersal, and then released to produce random walk-like trajectories. Serotonergic axons appear to show some of these properties.

the fibers enter the telencephalon. Hypothetically, the attracting cue may be a diffusing factor (which, if released by the dorsal pallium, could reach the habenula). These potential gradients have not yet been investigated experimentally or in computer simulations.

The *stochastic* component may be fundamental to the understanding of the apparently complex distribution patterns of serotonergic fibers in different vertebrate species. We have previously shown that the trajectories of serotonergic axons can be modeled as paths of FBM, a continuous-time stochastic process that evolves in space (Janušonis et al., 2020). We also have demonstrated in a supercomputing simulation that simulated FBM-fibers, walking in a geometric shape based on the mouse brain, produce fiber densities that approximate the actual serotonergic fiber densities, with no guiding cues (Janušonis et al., 2023). This result is partly due to a key mathematical property of FBM-fibers, their tendency to accumulate at the shape boundaries (Guggenberger et al., 2019; Vojta et al., 2020). An increased accumulation of serotonergic fibers at the pial and ventricular boundaries has been described by many studies in various brain regions across vertebrate species, but has been interpreted as a neuroanatomical region-specific feature (Martin et al., 1985; Mize and Horner, 1989; Dinopoulos and Dori, 1995; Morin and Meyer-Bernstein, 1999; Bjarkam et al., 2003, 2005; Awasthi et al., 2021; Bhat and Ganesh, 2023). Interestingly, this effect becomes even more pronounced in mice that lack protocadherin-αC2, a cell adhesion protein that is thought to support serotonergic fiber dispersion through self-avoidance (Katori et al., 2009; Katori et al., 2017). Additionally, FBM-trajectories have long-term "memory": each new step is a random event, but it correlates with the previous steps (history) of the fiber, including its possible reflections at the boundary. Therefore, the three-dimensional geometry of the brain becomes an important factor in the spatial distribution of fiber densities. Other research shows that brain function may be influenced

by brain geometry (Gjorevski et al., 2022; Pang et al., 2023). Spatial effects may also underlie a number of fundamental patterns that have come into focus only recently. For example, studies have demonstrated strong similarities in neocortical dynamics across mammalian species (Mahon, 2024) and a universal laminar distribution pattern of the power of cortical oscillations across primate neocortical areas (Mendoza-Halliday et al., 2024).

4.3 Stochasticity and determinism in axon development: insights and challenges

The supercomputing simulation of this study is a significant step in efforts to achieve a deeper understanding of the self-organization of serotonergic fibers. It is the first computational simulation of serotonergic fibers in a non-mammalian brain and it complements our recent supercomputing simulations in the mouse brain (Janušonis et al., 2020; Janušonis et al., 2023). The obtained results show strong similarity to the biological densities of serotonergic fibers and, in particular, highlight the universal tendency of serotonergic fibers to accumulate near tissue boundaries. This simulation does not include deterministic forces (e.g., axon-guiding gradients) which would require a considerable extension of the model, with limited biological information. In an interdisciplinary collaboration, we are currently developing the theory of FBM to incorporate other biologically-relevant elements, such as heterogeneous environments (Wang et al., 2023) and population-induced forces (House et al., 2025).

An interesting possibility exists that some oriented paths of serotonergic fibers are not due to guiding gradients but to the tendency of these fibers to opportunistically travel along major

(non-serotonergic) axon tracts. The propensity of serotonergic axons to adhere to many functionally diverse tracts, such as the medial forebrain bundle (Nieuwenhuys et al., 1982) or the fasciculus retroflexus (Beretta et al., 2012), has been noted in early studies and named "epiphytic guidance" (Lidov and Molliver, 1982; Wallace and Lauder, 1983; Jacobs and Azmitia, 1992), in reference to plant epiphytes (plants that grow on other plants for physical support). Indeed, in shark brains serotonergic fibers could travel along several tracts connecting the diencephalon and telencephalon, such as the tractus pallii or the fasciculus basalis telencephali (Smeets et al., 1983; Smeets, 1998; Hofmann and Northcutt, 2012). Likewise, serotonergic fibers could approach the habenula along the fasciculus retroflexus (Giuliani et al., 2002), as they do in mammalian brains (Jacobs and Azmitia, 1992). In an extreme case, serotonergic fibers could remain entirely stochastic but accumulate around the borders of these tracts, producing an illusion of oriented movement in population-level imaging. However, some individual serotonergic fibers are strongly oriented (Figure 6B), which suggests that this explanation is insufficient.

Even in the absence of guiding gradients, the simulation produced a strong accumulation of FBM-fibers in the inferior lobe of the hypothalamus (Figure 10D), the habenula (Figure 10D), and the dorsal pallium (Figure 10K), due to their high-curvature contours (Janušonis et al., 2020; Vojta et al., 2020). Some studies have suggested that serotonin itself may stimulate the growth of serotonergic fibers (Azmitia and Whitaker-Azmitia, 1991; Whitaker-Azmitia, 2001). Therefore, these high-density areas can induce a previously absent attracting force, affecting further fiber development. However, this information remains incomplete and sometimes contradictory, with opposite (negative feedback) effects of serotonin also reported (Nishiyama et al., 2002; Kornum et al., 2006; Daubert et al., 2010; Migliarini et al., 2013; Vicenzi et al., 2021; Nazzi et al., 2024).

No detectable border accumulation of serotonergic fibers is present in some angelshark brainstem regions, such as the tectum, perhaps because of frequent reflecting or adhesion events induced by densely packed axon tracts (not necessarily traveling in the same orientation). In theoretical studies, unexpected effects have been observed in particles undergoing FBM motion in heterogeneous, randomly structured environments (Wang et al., 2020). Also, the angelshark cerebellum was almost devoid of serotonergic fibers. This observation is consistent with the low density of serotonergic fibers in the mouse cerebellum (Awasthi et al., 2021). The cerebellum is a highly specialized structure, including its enormous number of granule cells, and may present an otherwise less permissive environment for serotonergic fibers. It may also be less physically accessible because of the dense axon tracts connecting it to the medulla (e.g., the cerebellar peduncles in mammals) (Smeets et al., 1983; Smeets, 1998; Montgomery et al., 2012).

Generally, the "flow" of serotonergic fibers in the angelshark forebrain was similar to that of the smallspotted catshark (Carrera et al., 2008). This sequence of fiber progression, in turn, shared considerable similarity with the development of serotonergic axons in the rat brain (Wallace and Lauder, 1983), despite major cytoarchitectonic differences and mammal-specific specializations.

For the purpose of this study, serotonergic fibers were treated as virtually identical in their properties. Recent single-cell RNA-seq studies have revealed an enormous transcriptional diversity of serotonergic neurons (Okaty et al., 2019; Ren et al., 2019; Okaty et al., 2020). These studies represent a major inflection in the field. However, it remains unknown if the same neuron can switch among several transcriptional programs ("attractors"), depending on its environment (Okaty et al., 2019). It is also unknown whether the current transcriptional program selected by the neuron depends on the path and history of its axon.

5 Conclusion

In conclusion, we note that the development of many, if not all, axon systems may depend on a dynamic interplay between a mathematically-definable stochastic process and constraining deterministic forces, *at all developmental times* (Figure 12). Due to the inherent properties of growth cones (Katz et al., 1984; Maskery and Shinbrot, 2005; Betz et al., 2006; Forghani et al., 2023), axons will tend to produce stochastic trajectories. However, it can result in a rich behavioral repertoire, as axons interact with their physical environment (tissue boundaries, physical obstacles, viscoelastic heterogeneities) and with each other. "Strategically placed" guiding factors (e.g., chemical gradients) are necessary to achieve the genetically predetermined wiring, but they may harness rather than suppress this inherent stochasticity. The depth and richness of such interactions is only beginning to be revealed, with implications for the self-organization, plasticity, and repair of nervous systems.

Data availability statement

The datasets used in this study can be found in the Dryad online repository at: https://datadryad.org/dataset/doi:10.5061/dryad.bk3j9kdpg.

Ethics statement

The animal study was approved by the UCSB Institutional Animal Care and Use Committee. The study was conducted in accordance with the local legislation and institutional requirements.

Author contributions

Funding

Acknowledgments

Conflict of interest

The authors declare that the research was conducted in the absence of any commercial or financial relationships that could be construed as a potential conflict of interest.

Generative AI statement

The authors declare that no Generative AI was used in the creation of this manuscript.

Publisher's note

All claims expressed in this article are solely those of the authors and do not necessarily represent those of their affiliated organizations, or those of the publisher, the editors and the reviewers. Any product that may be evaluated in this article, or claim that may be made by its manufacturer, is not guaranteed or endorsed by the publisher.

Supplementary material

The Supplementary Material for this article can be found online at: https://www.frontiersin.org/articles/10.3389/fnins.2025.1602116/full#supplementary-material

SUPPLEMENTARY FIGURES 1–8
High-resolution (tiled) images of serotonergic fibers at eight coronal levels of the Pacific angelshark telencephalon (corresponding to panels Figures 5A–H). The sections were immunostained for serotonin (5-HT) with the Cy3 fluorophore and imaged in color with a 5× objective.

References

Aitken, A. R., and Tork, I. (1988). Early development of serotonin-containing neurons and pathways as seen in wholemount preparations of the fetal rat brain. *J. Comp. Neurol.* 274, 32–47. doi: 10.1002/cne.902740105

Andrews, P. W., Bosyj, C., Brenton, L., Green, L., Gasser, P. J., Lowry, C. A., et al. (2022). All the brain's a stage for serotonin: The forgotten story of serotonin diffusion across cell membranes. *Proc. Biol. Sci.* 289:20221565. doi: 10.1098/rspb.2022.1565

Antonovaite, N., Hulshof, L. A., Hol, E. M., Wadman, W. J., and Iannuzzi, D. (2021). Viscoelastic mapping of mouse brain tissue: Relation to structure and age. *J. Mech. Behav. Biomed. Mater.* 113:104159. doi: 10.1016/j.jmbbm.2020.104159

Awasthi, J. R., Tamada, K., Overton, E. T. N., and Takumi, T. (2021). Comprehensive topographical map of the serotonergic fibers in the male mouse brain. *J. Comp. Neurol.* 529, 1391–1429. doi: 10.1002/cne.25027

Azmitia, E. C., and Whitaker-Azmitia, P. M. (1991). Awakening the sleeping giant: anatomy and plasticity of the brain serotonergic system. *J. Clin. Psychiatry* 52, 4–16.

Azmitia, E., and Gannon, P. (1983). The ultrastructural localization of serotonin immunoreactivity in myelinated and unmyelinated axons within the medial forebrain bundle of rat and monkey. *J. Neurosci.* 3, 2083–2090. doi: 10.1523/jneurosci.03-10-02083.1983

Barca, A., Vacca, F., Vizioli, J., Drago, F., Vetrugno, C., Verri, T., et al. (2017). Molecular and expression analysis of the Allograft inflammatory factor 1 (AIF-1) in the coelomocytes of the common sea urchin *Paracentrotus lividus*. *Fish. Shellfish. Immunol.* 71, 136–143. doi: 10.1016/j.fsi.2017.09.078

Beretta, C. A., Dross, N., Guiterrez-Triana, J. A., Ryu, S., and Carl, M. (2012). Habenula circuit development: past, present, and future. *Front. Neurosci.* 6:51. doi: 10.3389/fnins.2012.00051

Betz, T., Lim, D., and Käs, J. A. (2006). Neuronal growth: A bistable stochastic process. *Phys. Rev. Lett.* 96:098103. doi: 10.1103/PhysRevLett.96.098103

Bhat, S. K., and Ganesh, C. B. (2023). Organization of serotonergic system in *Sphaerotheca breviceps* (Dicroglossidae) tadpole brain. *Cell Tissue Res.* 391, 67–86. doi: 10.1007/s00441-022-03709-7

Biagini, F., Hu, Y., Øksendal, B., and Zhang, T. (2010). *Stochastic Calculus for Fractional Brownian Motion and Applications*. London: Springer.

Bifari, F., Decimo, I., Pino, A., Llorens-Bobadilla, E., Zhao, S., Lange, C., et al. (2017). Neurogenic radial glia-like cells in meninges migrate and differentiate into functionally integrated neurons in the neonatal cortex. *Cell. Stem. Cell.* 20, 360–373.e367. doi: 10.1016/j.stem.2016.10.020.

Biradar, A., and Ganesh, C. B. (2024). Serotonin-immunoreactivity in the brain of the cichlid fish *Oreochromis mossambicus*. *Anat. Rec (Hoboken).* 307, 320–344. doi: 10.1002/ar.25204

Bjarkam, C. R., Sørensen, J. C., and Geneser, F. A. (2003). Distribution and morphology of serotonin-immunoreactive axons in the hippocampal region of the New Zealand white rabbit. I. Area dentata and hippocampus. *Hippocampus* 13, 21–37. doi: 10.1002/hipo.10042

Bjarkam, C. R., Sørensen, J. C., and Geneser, F. A. (2005). Distribution and morphology of serotonin-immunoreactive axons in the retrohippocampal areas of the New Zealand white rabbit. *Anat. Embryol.* 210, 199–207. doi: 10.1007/s00429-005-0004-x

Blumenfeld, H. (2022). *Neuroanatomy Through Clinical Cases*, 3rd Edn. New York: Oxford University Press.

Bockaert, J., Claeysen, S., Bécamel, C., Dumuis, A., and Marin, P. (2006). Neuronal 5-HT metabotropic receptors: fine-tuning of their structure, signaling, and roles in synaptic modulation. *Cell Tissue Res.* 326, 553–572. doi: 10.1007/s00441-006-0286-1

Butler, A. B., and Hodos, W. (2005). *Comparative Vertebrate Neuroanatomy*, 2nd Edn. Hoboken, NJ: Wiley-Interscience.

Carrera, I., Molist, P., Anadon, R., and Rodriguez-Moldes, I. (2008). Development of the serotoninergic system in the central nervous system of a shark, the lesser spotted dogfish *Scyliorhinus canicula*. *J. Comp. Neurol.* 511, 804–831. doi: 10.1002/cne.21857

Cazettes, F., Reato, D., Morais, J. P., Renart, A., and Mainen, Z. F. (2021). Phasic activation of dorsal raphe serotonergic neurons increases pupil size. *Curr. Biol.* 31, 192–197.e194. doi: 10.1016/j.cub.2020.09.090.

Chaudhuri, O., Cooper-White, J., Janmey, P. A., Mooney, D. J., and Shenoy, V. B. (2020). Effects of extracellular matrix viscoelasticity on cellular behaviour. *Nature* 584, 535–546. doi: 10.1038/s41586-020-2612-2

Chen, W. V., Nwakeze, C. L., Denny, C. A., O'Keeffe, S., Rieger, M. A., Mountoufaris, G., et al. (2017). Pcdhαc2 is required for axonal tiling and assembly of serotonergic circuitries in mice. *Science* 356, 406–411. doi: 10.1126/science.aal3231

Cheung, A., Konno, K., Imamura, Y., Matsui, A., Abe, M., Sakimura, K., et al. (2023). Neurexins in serotonergic neurons regulate neuronal survival, serotonin transmission, and complex mouse behaviors. *Elife* 12:e085058. doi: 10.7554/eLife.85058

Compagno, L., Dando, M., and Sarah, F. (2005). *Sharks of the World*. Princeton and Oxford: Princeton University Press.

Cooke, P., Janowitz, H., and Dougherty, S. E. (2022). Neuronal redevelopment and the regeneration of neuromodulatory axons in the adult mammalian central nervous system. *Front. Cell. Neurosci.* 16:872501. doi: 10.3389/fncel.2022.872501

Daubert, E. A., Heffron, D. S., Mandell, J. W., and Condron, B. G. (2010). Serotonergic dystrophy induced by excess serotonin. *Mol. Cell. Neurosci.* 44, 297–306. doi: 10.1016/j.mcn.2010.04.001

de Bellard, M. E. (2016). Myelin in cartilaginous fish. *Brain Res.* 1641, 34–42. doi: 10.1016/j.brainres.2016.01.013

Dey, S., Surendran, D., Engberg, O., Gupta, A., Fanibunda, S. E., Das, A., et al. (2021). Altered membrane mechanics provides a receptor-independent pathway for serotonin action. *Chemistry* 27, 7533–7541. doi: 10.1002/chem.202100328

Dinopoulos, A., and Dori, I. (1995). The development of the serotonergic fiber network of the lateral ventricles of the rat brain: A light and electron microscopic immunocytochemical analysis. *Exp. Neurol.* 133, 73–84. doi: 10.1006/exnr.1995.1009

Dohare, S., Hernandez-Garcia, J. F., Lan, Q., Rahman, P., Mahmood, A. R., and Sutton, R. S. (2024). Loss of plasticity in deep continual learning. *Nature* 632, 768–774. doi: 10.1038/s41586-024-07711-7

Donovan, L. J., Spencer, W. C., Kitt, M. M., Eastman, B. A., Lobur, K. J., Jiao, K., et al. (2019). Lmx1b is required at multiple stages to build expansive serotonergic axon architectures. *Elife* 8:e48788. doi: 10.7554/eLife.48788

Ebbesson, L. O., Holmqvist, B., Ostholm, T., and Ekström, P. (1992). Transient serotonin-immunoreactive neurons coincide with a critical period of neural development in coho salmon (*Oncorhynchus kisutch*). *Cell. Tissue Res.* 268, 389–392. doi: 10.1007/bf00318807

Flood, D. C., Engel, D. L., Simon, C. C., Negherbon, K. R., Murphy, L. J., Tamavimok, W., et al. (2012). Brain growth trajectories in mouse strains with central and peripheral serotonin differences: Relevance to autism models. *Neuroscience* 210, 286–295. doi: 10.1016/j.neuroscience.2012.03.010

Fonseca, E. M., Noronha-de-Souza, C. R., Bícego, K. C., Branco, L. G. S., and Gargaglioni, L. H. (2021). 5-HT neurons of the medullary raphe contribute to respiratory control in toads. *Respir. Physiol. Neurobiol.* 293:103717. doi: 10.1016/j.resp.2021.103717

Forghani, R., Chandrasekaran, A., Papoian, G., and Giniger, E. (2023). A new view of axon growth and guidance grounded in the stochastic dynamics of actin networks. *Open Biol.* 13:220359. doi: 10.1098/rsob.220359

Fujita, T., Aoki, N., Mori, C., Homma, K. J., and Yamaguchi, S. (2023). Molecular biology of serotonergic systems in avian brains. *Front. Mol. Neurosci.* 16:1226645. doi: 10.3389/fnmol.2023.1226645

Furness, J. B., and Stebbing, M. J. (2018). The first brain: Species comparisons and evolutionary implications for the enteric and central nervous systems. *Neurogastroenterol. Motil.* 30:e13234. doi: 10.1111/nmo.13234

Gershon, M. D., and Margolis, K. G. (2021). The gut, its microbiome, and the brain: connections and communications. *J. Clin. Invest.* 131:e143768. doi: 10.1172/jci143768

Gianni, G., and Pasqualetti, M. (2023). Wiring and volume transmission: An overview of the dual modality for serotonin neurotransmission. *ACS Chem. Neurosci.* 14, 4093–4104. doi: 10.1021/acschemneuro.3c00648

Giuliani, A., Minelli, D., Quaglia, A., and Villani, L. (2002). Telencephalo-habenulo-interpeduncular connections in the brain of the shark *Chiloscyllium arabicum*. *Brain Res.* 926, 186–190. doi: 10.1016/s0006-8993(01)03310-8

Gjorevski, N., Nikolaev, M., Brown, T. E., Mitrofanova, O., Brandenberg, N., DelRio, F. W., et al. (2022). Tissue geometry drives deterministic organoid patterning. *Science* 375:eaaw9021. doi: 10.1126/science.aaw9021

Guggenberger, T., Pagnini, G., Vojta, T., and Metzler, R. (2019). Fractional Brownian motion in a finite interval: correlations effect depletion or accretion zones of particles near boundaries. *New J. Phys.* 21:022002. doi: 10.1088/1367-2630/ab075f

Hawthorne, A. L., Hu, H., Kundu, B., Steinmetz, M. P., Wylie, C. J., Deneris, E. S., et al. (2011). The unusual response of serotonergic neurons after CNS injury: Lack of axonal dieback and enhanced sprouting within the inhibitory environment of the glial scar. *J. Neurosci.* 31, 5605–5616. doi: 10.1523/jneurosci.6663-10.2011

Hingorani, M., Viviani, A. M. L., Sanfilippo, J. E., and Janušonis, S. (2022). High-resolution spatiotemporal analysis of single serotonergic axons in an in vitro system. *Front. Neurosci.* 16:994735. doi: 10.3389/fnins.2022.994735

Hofmann, M. H., and Northcutt, R. G. (2012). Forebrain organization in elasmobranchs. *Brain Behav. Evol.* 80, 142–151. doi: 10.1159/000339874

Hornung, J. P. (2003). The human raphe nuclei and the serotonergic system. *J. Chem. Neuroanat.* 26, 331–343. doi: 10.1016/j.jchemneu.2003.10.002

House, J., Janušonis, S., Metzler, R., and Vojta, T. (2025). Fractional Brownian motion with mean-density interaction. *arXiv [Preprint]* doi: 10.48550/arXiv.2503.15255

Jacobs, B. L., and Azmitia, E. C. (1992). Structure and function of the brain serotonin system. *Physiol. Rev.* 72, 165–229. doi: 10.1152/physrev.1992.72.1.165

Janušonis, S. (2018). Some galeomorph sharks express a mammalian microglia-specific protein in radial ependymoglia of the telencephalon. *Brain Behav. Evol.* 91, 17–30. doi: 10.1159/000484196

Janušonis, S., and Detering, N. (2019). A stochastic approach to serotonergic fibers in mental disorders. *Biochimie* 161, 15–22. doi: 10.1016/j.biochi.2018.07.014

Janušonis, S., Detering, N., Metzler, R., and Vojta, T. (2020). Serotonergic axons as fractional Brownian motion paths: Insights into the self-organization of regional densities. *Front. Comput. Neurosci.* 14:56. doi: 10.3389/fncom.2020.00056

Janušonis, S., Gluncic, V., and Rakic, P. (2004). Early serotonergic projections to Cajal-Retzius cells: Relevance for cortical development. *J. Neurosci.* 24, 1652–1659. doi: 10.1523/jneurosci.4651-03.2004

Janušonis, S., Haiman, J. H., Metzler, R., and Vojta, T. (2023). Predicting the distribution of serotonergic axons: A supercomputing simulation of reflected fractional Brownian motion in a 3D-mouse brain model. *Front. Comput. Neurosci.* 17:1189853. doi: 10.3389/fncom.2023.1189853

Jin, Y., Dougherty, S. E., Wood, K., Sun, L., Cudmore, R. H., Abdalla, A., et al. (2016). Regrowth of serotonin axons in the adult mouse brain following injury. *Neuron* 91, 748–762. doi: 10.1016/j.neuron.2016.07.024

Jordan, J. E. L., Bertalan, G., Meyer, T., Tzschätzsch, H., Gauert, A., Bramè, L., et al. (2022). Microscopic multifrequency MR elastography for mapping viscoelasticity in zebrafish. *Magn. Reson. Med.* 87, 1435–1445. doi: 10.1002/mrm.29066

Kajstura, T. J., Dougherty, S. E., and Linden, D. J. (2018). Serotonin axons in the neocortex of the adult female mouse regrow after traumatic brain injury. *J. Neurosci. Res.* 96, 512–526. doi: 10.1002/jnr.24059

Katori, S., Hamada, S., Noguchi, Y., Fukuda, E., Yamamoto, T., Yamamoto, H., et al. (2009). Protocadherin-α family is required for serotonergic projections to appropriately innervate target brain areas. *J. Neurosci.* 29, 9137–9147. doi: 10.1523/jneurosci.5478-08.2009

Katori, S., Noguchi-Katori, Y., Okayama, A., Kawamura, Y., Luo, W., Sakimura, K., et al. (2017). Protocadherin-αC2 is required for diffuse projections of serotonergic axons. *Sci. Rep.* 7:15908. doi: 10.1038/s41598-017-16120-y

Katz, M. J., George, E. B., and Gilbert, L. J. (1984). Axonal elongation as a stochastic walk. *Cell. Motil.* 4, 351–370. doi: 10.1002/cm.970040505

Kitt, M. M., Tabuchi, N., Spencer, W. C., Robinson, H. L., Zhang, X. L., Eastman, B. A., et al. (2022). An adult-stage transcriptional program for survival of serotonergic connectivity. *Cell. Rep.* 39:110711. doi: 10.1016/j.celrep.2022.110711

Kiyasova, V., and Gaspar, P. (2011). Development of raphe serotonin neurons from specification to guidance. *Eur. J. Neurosci.* 34, 1553–1562. doi: 10.1111/j.1460-9568.2011.07910.x

Kornum, B. R., Licht, C. L., Weikop, P., Knudsen, G. M., and Aznar, S. (2006). Central serotonin depletion affects rat brain areas differently: A qualitative and quantitative comparison between different treatment schemes. *Neurosci. Lett.* 392, 129–134. doi: 10.1016/j.neulet.2005.09.013

Lee, C., Zhang, Z., and Janušonis, S. (2022). Brain serotonergic fibers suggest anomalous diffusion-based dropout in artificial neural networks. *Front. Neurosci.* 16:949934. doi: 10.3389/fnins.2022.949934

Lesch, K. P., and Waider, J. (2012). Serotonin in the modulation of neural plasticity and networks: Implications for neurodevelopmental disorders. *Neuron* 76, 175–191. doi: 10.1016/j.neuron.2012.09.013

Lidov, H. G., and Molliver, M. E. (1982). An immunohistochemical study of serotonin neuron development in the rat: Ascending pathways and terminal fields. *Brain Res. Bull.* 8, 389–430. doi: 10.1016/0361-9230(82)90077-6

Lillesaar, C. (2011). The serotonergic system in fish. *J. Chem. Neuroanat.* 41, 294–308. doi: 10.1016/j.jchemneu.2011.05.009

López-Romero, F. A., Stumpf, S., Pfaff, C., Marramà, G., Johanson, Z., and Kriwet, J. (2020). Evolutionary trends of the conserved neurocranium shape in angel sharks (Squatiniformes. Elasmobranchii). *Sci. Rep.* 10:12582. doi: 10.1038/s41598-020-69525-7

Lozano, D., González, A., and López, J. M. (2020). Neuroanatomical distribution of the serotonergic system in the brain and retina of Holostean fishes, the sister group to Teleosts. *Brain Behav. Evol.* 95, 25–44. doi: 10.1159/000505473

MacDonnell, M. F. (1980). Cerebrospinal fluid contacting and supraependymal mesencephalic trigeminal cells in the blue and mako sharks. A scanning electron microscopic study. *Brain Behav. Evol.* 17, 164–177. doi: 10.1159/000121796

MacDonnell, M. F. (1983). Mesencephalic trigeminal midline ridge formation in sharks, a proposed circumventricular organ: developmental aspects. *Anat. Rec.* 206, 319–327. doi: 10.1002/ar.1092060311

MacDonnell, M. F. (1984). Circumventricular mesencephalic trigeminal midline ridge formation in cartilaginous fishes: Species variations. *Brain Behav. Evol.* 24, 124–134. doi: 10.1159/000121310

MacDonnell, M. F. (1989). Sub/supraependymal axonal net in the brains of sharks and probable targets in parasynaptic relationship. *Brain Behav. Evol.* 34, 201–211. doi: 10.1159/000116506

Mahon, S. (2024). Variation and convergence in the morpho-functional properties of the mammalian neocortex. *Front. Syst. Neurosci.* 18:1413780. doi: 10.3389/fnsys.2024.1413780

Maisey, J. G., Ehret, D. J., and Denton, J. S. S. (2020). A new genus of late Cretaceous angel shark (Elasmobranchii; Squatinidae), with comments on squatinid phylogeny. *Am. Museum Novitates* 3954, 1–29. doi: 10.1206/3954.1

Makse, H. A., Havlin, S., Schwartz, M., and Stanley, H. E. (1996). Method for generating long-range correlations for large systems. *Phys. Rev. E* 53, 5445–5449. doi: 10.1103/PhysRevE.53.5445

Mamounas, L. A., Blue, M. E., Siuciak, J. A., and Altar, C. A. (1995). Brain-derived neurotrophic factor promotes the survival and sprouting of serotonergic axons in rat brain. *J. Neurosci.* 15, 7929–7939. doi: 10.1523/JNEUROSCI.15-12-07929.1995

Mandelbrot, B. B., and Van Ness, J. W. (1968). Fractional Brownian motions, fractional noises and applications. *SIAM Rev.* 10, 422–437. doi: 10.1137/1010093

Manger, P. R., Fahringer, H. M., Pettigrew, J. D., and Siegel, J. M. (2002). The distribution and morphological characteristics of serotonergic cells in the brain of monotremes. *Brain Behav. Evol.* 60, 315–332. doi: 10.1159/000067194

Martin, G. F., DeLorenzo, G., Ho, R. H., Humbertson, A. O. Jr., and Waltzer, R. (1985). Serotonergic innervation of the forebrain in the North American opossum. *Brain Behav. Evol.* 26, 196–228. doi: 10.1159/000118776

Maskery, S., and Shinbrot, T. (2005). Deterministic and stochastic elements of axonal guidance. *Annu. Rev. Biomed. Eng.* 7, 187–221. doi: 10.1146/annurev.bioeng.7.060804.100446

Mays, K. C., Haiman, J. H., and Janušonis, S. (2023). An experimental platform for stochastic analyses of single serotonergic fibers in the mouse brain. *Front. Neurosci.* 17:1241919. doi: 10.3389/fnins.2023.1241919

McCormick, H. W., Allen, T., and Young, W. E. (1963). *Shadows in the Sea: The Sharks, Skates and Rays.* New York: Weathervane Books.

Mendoza-Halliday, D., Major, A. J., Lee, N., Lichtenfeld, M. J., Carlson, B., Mitchell, B., et al. (2024). A ubiquitous spectrolaminar motif of local field potential power across the primate cortex. *Nat. Neurosci.* 27, 547–560. doi: 10.1038/s41593-023-01554-7

Migliarini, S., Pacini, G., Pelosi, B., Lunardi, G., and Pasqualetti, M. (2013). Lack of brain serotonin affects postnatal development and serotonergic neuronal circuitry formation. *Mol. Psychiatry* 18, 1106–1118. doi: 10.1038/mp.2012.128

Mize, R. R., and Horner, L. H. (1989). Origin, distribution, and morphology of serotonergic afferents to the cat superior colliculus: A light and electron microscope immunocytochemistry study. *Exp. Brain Res.* 75, 83–98. doi: 10.1007/bf00248533

Montalbano, A., Waider, J., Barbieri, M., Baytas, O., Lesch, K. P., Corradetti, R., et al. (2015). Cellular resilience: 5-HT neurons in Tph2(-/-) mice retain normal firing behavior despite the lack of brain 5-HT. *Eur. Neuropsychopharmacol.* 25, 2022–2035. doi: 10.1016/j.euroneuro.2015.08.021

Montgomery, J. C., Bodznick, D., and Yopak, K. E. (2012). The cerebellum and cerebellum-like structures of cartilaginous fishes. *Brain Behav. Evol.* 80, 152–165. doi: 10.1159/000339868

Morin, L. P., and Meyer-Bernstein, E. L. (1999). The ascending serotonergic system in the hamster: Comparison with projections of the dorsal and median raphe nuclei. *Neuroscience* 91, 81–105. doi: 10.1016/s0306-4522(98)00585-5

Mosienko, V., Beis, D., Pasqualetti, M., Waider, J., Matthes, S., Qadri, F., et al. (2015). Life without brain serotonin: Reevaluation of serotonin function with mice deficient in brain serotonin synthesis. *Behav. Brain Res.* 277, 78–88. doi: 10.1016/j.bbr.2014.06.005

Nazzi, S., Maddaloni, G., Pratelli, M., and Pasqualetti, M. (2019). Fluoxetine induces morphological rearrangements of serotonergic fibers in the hippocampus. *ACS Chem. Neurosci.* 10, 3218–3224. doi: 10.1021/acschemneuro.8b00655

Nazzi, S., Picchi, M., Migliarini, S., Maddaloni, G., Barsotti, N., and Pasqualetti, M. (2024). Reversible morphological remodeling of prefrontal and hippocampal serotonergic fibers by fluoxetine. *ACS Chem. Neurosci.* 15, 1702–1711. doi: 10.1021/acschemneuro.3c00837

New, J. G. (2001). Comparative neurobiology of the elasmobranch cerebellum: Theme and variations on a sensorimotor interface. *Environ. Biol. Fish.* 60, 93–108. doi: 10.1023/A:1007631405904

Nieuwenhuys, R., Geeraedts, L. M., and Veening, J. G. (1982). The medial forebrain bundle of the rat. I. General introduction. *J. Comp. Neurol.* 206, 49–81. doi: 10.1002/cne.902060106

Nishiyama, H., Takemura, M., Takeda, T., and Itohara, S. (2002). Normal development of serotonergic neurons in mice lacking S100B. *Neurosci. Lett.* 321, 49–52. doi: 10.1016/s0304-3940(01)02549-6

Ogelman, R., Gomez Wulschner, L. E., Hoelscher, V. M., Hwang, I. W., Chang, V. N., and Oh, W. C. (2024). Serotonin modulates excitatory synapse maturation in the developing prefrontal cortex. *Nat. Commun.* 15:1368. doi: 10.1038/s41467-024-45734-w

Okaty, B. W., Commons, K. G., and Dymecki, S. M. (2019). Embracing diversity in the 5-HT neuronal system. *Nat. Rev. Neurosci.* 20, 397–424. doi: 10.1038/s41583-019-0151-3

Okaty, B. W., Sturrock, N., Escobedo Lozoya, Y., Chang, Y., Senft, R. A., Lyon, K. A., et al. (2020). A single-cell transcriptomic and anatomic atlas of mouse dorsal raphe Pet1 neurons. *Elife* 9:e55523. doi: 10.7554/eLife.55523

Page, C. E., Epperson, C. N., Novick, A. M., Duffy, K. A., and Thompson, S. M. (2024). Beyond the serotonin deficit hypothesis: Communicating a neuroplasticity framework of major depressive disorder. *Mol. Psychiatry* 29, 3802–3813. doi: 10.1038/s41380-024-02625-2

Pandya, D. N., Seltzer, B., Petrides, M., and Cipolloni, P. B. (2015). *Cerebral Cortex: Architecture, Connections, and the Dual Origin Concept.* Oxford: Oxford University Press.

Pang, J. C., Aquino, K. M., Oldehinkel, M., Robinson, P. A., Fulcher, B. D., Breakspear, M., et al. (2023). Geometric constraints on human brain function. *Nature* 618, 566–574. doi: 10.1038/s41586-023-06098-1

Papadopoulos, G. C., Parnavelas, J. G., and Buijs, R. (1987). Monoaminergic fibers form conventional synapses in the cerebral cortex. *Neurosci. Lett.* 76, 275–279. doi: 10.1016/0304-3940(87)90414-9

Parent, A. (1981). Comparative anatomy of the serotoninergic systems. *J. Physiol.* 77, 147–156.

Paxinos, G., Kassem, M. S., and Kirkcaldie, M. (2022). *Chemoarchitectonic Atlas of the Rat Brain.* London: Academic Press.

Qian, H. (2003). "Fractional Brownian motion and fractional Gaussian noise," in *Processes with Long-Range Correlations: Theory and Applications*, eds G. Rangarajan and M. Ding (Berlin: Springer), 22–33.

Ren, J., Friedmann, D., Xiong, J., Liu, C. D., Ferguson, B. R., Weerakkody, T., et al. (2018). Anatomically defined and functionally distinct dorsal raphe serotonin sub-systems. *Cell* 175, 472–487.e420. doi: 10.1016/j.cell.2018.07.043

Ren, J., Isakova, A., Friedmann, D., Zeng, J., Grutzner, S. M., Pun, A., et al. (2019). Single-cell transcriptomes and whole-brain projections of serotonin neurons in the mouse dorsal and median raphe nuclei. *Elife* 8:e49424. doi: 10.7554/eLife.49424

Rizzo, D. J., White, J. D., Spedden, E., Wiens, M. R., Kaplan, D. L., Atherton, T. J., et al. (2013). Neuronal growth as diffusion in an effective potential. *Phys. Rev. E Stat. Nonlin. Soft. Matter. Phys.* 88:042707. doi: 10.1103/PhysRevE.88.042707

Roberts, B. L., and Witkovsky, P. (1975). A functional analysis of the mesencephalic nucleus of the fifth nerve in the selachian brain. *Proc. R. Soc. Lond. B Biol. Sci.* 190, 473–495. doi: 10.1098/rspb.1975.0107

Rodrigues, S. L., Maseko, B. C., Ihunwo, A. O., Fuxe, K., and Manger, P. R. (2008). Nuclear organization and morphology of serotonergic neurons in the brain of the Nile crocodile, *Crocodylus niloticus. J. Chem. Neuroanat.* 35, 133–145. doi: 10.1016/j.jchemneu.2007.08.007

Santos, T. E., Schaffran, B., Broguière, N., Meyn, L., Zenobi-Wong, M., and Bradke, F. (2020). Axon growth of CNS neurons in three dimensions is amoeboid and independent of adhesions. *Cell Rep.* 32:107907. doi: 10.1016/j.celrep.2020.107907

Shimada, T., Kohyama, K., Yoshida, T., and Yamagata, K. (2024). Neuritin controls axonal branching in serotonin neurons: A possible mediator involved in the regulation of depressive and anxiety behaviors via FGF signaling. *J. Neurosci.* 44:e0129232024. doi: 10.1523/jneurosci.0129-23.2024

Slaten, E. R., Hernandez, M. C., Albay, R. III, Lavian, R., and Janušonis, S. (2010). Transient expression of serotonin 5-HT$_4$ receptors in the mouse developing thalamocortical projections. *Dev. Neurobiol.* 70, 165–181. doi: 10.1002/dneu.20775

Smeets, W. J. A. J. (1998). "Cartilaginous Fishes," in *The Central Nervous System of Cartilaginous Fishes*, eds R. Nieuwenhuys, H. J. Ten Donkelaar, and C. Nicholson (Berlin: Springer-Verlag).

Smeets, W. J. A. J., Nieuwenhuys, R., and Roberts, B. L. (1983). *The Central Nervous System of Cartilaginous Fishes: Structure and Functional Correlations.* New York: Springer-Verlag.

Smiley, J. F., and Goldman-Rakic, P. S. (1996). Serotonergic axons in monkey prefrontal cerebral cortex synapse predominantly on interneurons as demonstrated by serial section electron microscopy. *J. Comp. Neurol.* 367, 431–443. doi: 10.1002/(sici)1096-9861(19960408)367:3<431::Aid-cne8>3.0.Co;2-6

Striedter, G. F., and Northcutt, R. G. (2020). *Brains Through Time.* New York: Oxford University Press.

Stuesse, S. L., Cruce, W. L., and Northcutt, R. G. (1991). Localization of serotonin, tyrosine hydroxylase, and leu-enkephalin immunoreactive cells in the brainstem of the horn shark, *Heterodontus francisci. J. Comp. Neurol.* 308, 277–292. doi: 10.1002/cne.903080211

Stuesse, S. L., Stuesse, D. C., and Cruce, W. L. (1995). Raphe nuclei in three cartilaginous fishes, *Hydrolagus colliei, Heterodontus francisci*, and *Squalus acanthias. J. Comp. Neurol.* 358, 414–427. doi: 10.1002/cne.903580308

Teissier, A., Soiza-Reilly, M., and Gaspar, P. (2017). Refining the role of 5-HT in postnatal development of brain circuits. *Front. Cell. Neurosci.* 11:139. doi: 10.3389/fncel.2017.00139

Verkhratsky, A., Arranz, A. M., Ciuba, K., and Pękowska, A. (2022). Evolution of neuroglia. *Ann. N. Y. Acad. Sci.* 1518, 120–130. doi: 10.1111/nyas.14917

Vertes, R. P. (1991). A PHA-L analysis of ascending projections of the dorsal raphe nucleus in the rat. *J. Comp. Neurol.* 313, 643–668. doi: 10.1002/cne.903130409

Vertes, R. P., Fortin, W. J., and Crane, A. M. (1999). Projections of the median raphe nucleus in the rat. *J. Comp. Neurol.* 407, 555–582.

Vicenzi, S., Foa, L., and Gasperini, R. J. (2021). Serotonin functions as a bidirectional guidance molecule regulating growth cone motility. *Cell. Mol. Life Sci.* 78, 2247–2262. doi: 10.1007/s00018-020-03628-2

Voigt, T., and de Lima, A. D. (1991). Serotoninergic innervation of the ferret cerebral cortex. II. Postnatal development. *J. Comp. Neurol.* 314, 415–428. doi: 10.1002/cne.903140215

Vojta, T., Halladay, S., Skinner, S., Janušonis, S., Guggenberger, T., and Metzler, R. (2020). Reflected fractional Brownian motion in one and higher dimensions. *Phys. Rev. E* 102:032108. doi: 10.1103/PhysRevE.102.032108

Wada, A. H. O., and Vojta, T. (2018). Fractional Brownian motion with a reflecting wall. *Phys. Rev. E* 97:020102. doi: 10.1103/PhysRevE.97.020102

Wake, H., Moorhouse, A. J., Jinno, S., Kohsaka, S., and Nabekura, J. (2009). Resting microglia directly monitor the functional state of synapses in vivo and determine the fate of ischemic terminals. *J. Neurosci.* 29, 3974–3980. doi: 10.1523/jneurosci.4363-08.2009

Wallace, J. A., and Lauder, J. M. (1983). Development of the serotonergic system in the rat embryo: An immunocytochemical study. *Brain Res. Bull.* 10, 459–479. doi: 10.1016/0361-9230(83)90144-2

Wang, W., Balcerek, M., Burnecki, K., Chechkin, A. V., Janušonis, S., Ślęzak, J., et al. (2023). Memory-multi-fractional Brownian motion with continuous correlations. *Phys. Rev. Res.* 5:L032025. doi: 10.1103/PhysRevResearch.5.L032025

Wang, W., Seno, F., Sokolov, I. M., Chechkin, A. V., and Metzler, R. (2020). Unexpected crossovers in correlated random-diffusivity processes. *N. J. Phys.* 22:083041. doi: 10.1088/1367-2630/aba390

Westlund, K. N., Lu, Y., Coggeshall, R. E., and Willis, W. D. (1992). Serotonin is found in myelinated axons of the dorsolateral funiculus in monkeys. *Neurosci. Lett.* 141, 35–38. doi: 10.1016/0304-3940(92)90328-5

Whitaker-Azmitia, P. M. (2001). Serotonin and brain development: Role in human developmental diseases. *Brain Res. Bull.* 56, 479–485. doi: 10.1016/s0361-9230(01)00615-3

Witkovsky, P., and Roberts, B. L. (1975). The light microscopical structure of the mesencephalic nucleus of the fifth nerve in the selachian brain. *Proc. R. Soc. Lond. B Biol. Sci.* 190, 457–471. doi: 10.1098/rspb.1975.0106

Witkovsky, P., and Roberts, B. L. (1976). Electron microscopic observations of the mesencephalic nucleus of the fifth nerve in the Selachian brain. *J. Neurocytol.* 5, 643–660. doi: 10.1007/bf01181578

Yip, P. K., Schmitzberger, M., Al-Hasan, M., George, J., Tripoliti, E., Michael-Titus, A. T., et al. (2020). Serotonin expression in the song circuitry of adult male zebra finches. *Neuroscience* 444, 170–182. doi: 10.1016/j.neuroscience.2020.06.018

Yopak, K. E. (2012). Neuroecology of cartilaginous fishes: The functional implications of brain scaling. *J. Fish. Biol.* 80, 1968–2023. doi: 10.1111/j.1095-8649.2012.03254.x

Yopak, K. E., McMeans, B. C., Mull, C. G., Feindel, K. W., Kovacs, K. M., Lydersen, C., et al. (2019). Comparative brain morphology of the Greenland and Pacific sleeper sharks and its functional implications. *Sci. Rep.* 9:10022. doi: 10.1038/s41598-019-46225-5

Zalc, B. (2016). The acquisition of myelin: An evolutionary perspective. *Brain Res.* 1641, 4–10. doi: 10.1016/j.brainres.2015.09.005

Zhang, Y., Zhang, P., Shin, M., Chang, Y., Abbott, S. B. G., Venton, B. J., et al. (2025). Coding principles and mechanisms of serotonergic transmission modes. *Mol. Psychiatry* doi: 10.1038/s41380-025-02930-4 Online ahead of print.